ALANINE, ASPARTIC ACID AND LACTOSE-CAPPED CuS, ZnS and FeS NANOPARTICLES: SYNTHESIS, CHARACTERIZATION AND PROPERTIES

---

by

THAPELO PRINCE MOFOKENG

(211102741)

Thesis in fulfilment of the requirement for the degree

MAGISTER OF TECHNOLOGIAE

in

CHEMISTRY

in the

FACULTY OF APPLIED AND COMPUTER SCIENCES

of the

VAAL UNIVERSITY OF TECHNOLOGY

Supervisor: Prof MJ MOLOTO

Co-supervisors: Dr PM SHUMBULA

Academic year 2017

DECLARATION

I declare that the work presented in this dissertation was carried out by me under the supervision of Professor MJ Moloto and Doctor PM Shumbula. It is being submitted for the degree of Magister of Technologiae in the Vaal University of Technology, Vanderbijlpark, and has not been submitted before for any degree or examination at any other university.

T.P Mofokeng (211102741)

……Date:……...

Supervisor: Prof M.J. Moloto

……Date:…….

DEDICATION

For you my loving family

"The love that I have for you cannot be measured. May God bless you all."

ACKNOWLEDGEMENTS

In pursuit of this academic endeavour I feel that I have been fortunate with inspiration, guidance, direction, co-operation, love and care that all came in my way in abundance and it seems almost an impossible task for me to adequately thank everyone who has contributed to my successes.

I express my sincere thanks to my supervisor, **Professor Makwena Justice Moloto** for giving me the opportunity to conduct my research in his research group. My gratitude to him for his invaluable support and guidance during my study years can never be fully expressed. I appreciate the support and guidance you gave me.

I extend my sincere thanks to my co-supervisor, **Doctor Poslet Morgan Shumbula** for being such an inspiration to my life. He has not only been a supervisor but a true father and a role model to me. He has impacted positively in my life both academically and personally. As a supervisor, he believed in me even when I did not believe in myself. I would also like to thank him for showing confidence in me and my work. I appreciate the advices and support you gave me.

A special thanks to my friends and colleagues in our research group, the **nano-catalysis-adsorption-phytochemistry** (NCAP) in the department of chemistry. You guys were awesome to hang around with and I will always miss all the moments of laughter and sharing of knowledge and jokes.

I also gratefully acknowledge Mr Phumalani Tetyana for the help with XRD analysis and toxicity studies. Your patience with me was very superb.

A special thanks to my academic friends: Khumblani Mnqiwu, Wanda Bout, Thembinkosi Sibokoza, Themba Ntuli, Kopano Mokubung, Tankiso Masangane, Dilotsego Magaga and David Shooto. You all shape my life one way or another to be a success.

I am grateful of Vaal University of Technology and Mintek for allowing me to do my studies at your premises. A sincere thanks to VUT (Hub and Spokes funding) and NRF for their generous financial support. I would like to also thank everyone who has interacted with me one way or another during my academic development. Above all and everyone I thank **God** for directing my footstep. With God nothing could be impossible for me. To Him be all the glory.

PUBLICATIONS AND CONFERENCES

Publications

1. T.P Mofokeng, Girly Mabena, M. J. Moloto, P.M. Shumbula, P.K Mubiay, P. Nyamukamba. Temperature influence on the lactose capped metal sulphide nanoparticles. (2017). Chalcogenide Letters. 14(8), 347-355.
2. T.P Mofokeng, M. J. Moloto, P.M. Shumbula, P. Nyamukamba, P.K Mubiayi, S. Takaidza, L. Marais. Antimicrobial activity of amino acid capped zinc and copper sulphide nanoparticles, Journal of Nanobiotechnology, 2017, **accepted**.
3. K.F Chepape, T.P Mofokeng, P. Nyamukamba, K.P Mubiayi, M.J Moloto. Enhanced photocatalytic degradation of methyl blue using PVP-capped and uncapped CdSe nanoparticles, Journal of Nanotechnology, **accepted.**

Conferences and Symposia

- **Synthesis and characterization of alanine-capped water soluble CuS nanoparticles.** Oral presentation at South African Chemical Institute (SACI) young chemist symposium, University of South Africa (UNISA), November 2015. Johannesburg, South Africa.
- **Synthesis and characterization of alanine-capped water soluble CuS nanoparticles.** Poster presentation at South African Chemical Institute (SACI) convention, Annual conference, December 2015. Durban, South Africa.
- **Synthesis and characterization of alanine-capped water soluble ZnS nanoparticles.** Oral presentation at Vaal University of Technology 1st

postgraduate's interdisciplinary conference, November 2016. Sedibeng, South Africa.

- **Photocatalytic activity of alanine-capped water soluble ZnS.** Oral presentation at Environment, materials and green technology conference, Centre of renewable energy and water, Annual conference, November 2016. Sedibeng, South Africa.
- **Photocatalytic activity of alanine-capped water soluble ZnS.** Oral presentation at 13th International Conference on Nanotek and Expo, Phoenix, December 2016. Arizona, United States of America.

Abstract

Water soluble metal sulfide nanoparticles were successfully synthesized using an aqueous, simple and environmentally friendly synthetic method in the presence of L-alanine, L-aspartic acid and lactose, acting as both stabilizers and crystal growth modifiers. The structural and optical properties of the synthesized metal sulfide nanoparticles were characterized by X-ray diffraction (XRD), transmission electron microscopy (TEM), Fourier transform infrared (FTIR), Ultraviolet-visible (UV-Vis) and photoluminescence spectroscopy.

Colloidal method was employed in the synthesis of CuS, ZnS and FeS nanoparticles from metal chlorides as precursors and thioacetamide (TAA) as a sulphur source. The effect of temperature on the growth and solubility of nanoparticles was investigated. The absorption spectra of all samples prepared were blue shifted as compared to their bulk materials indicating small particles size. The morphologies and sizes of the nanoparticles were influenced by the variation of temperature and capping agent. TEM images revealed interesting changes in the morphology of CuS nanoparticles formed from various capping agents. By varying the temperature, L-aspartic acid-capped CuS nanoparticles changed from rod-shaped particles to particles dominated with hexagonal shape. However, the morphologies of both ZnS and FeS nanoparticles were close to spherical shape and were unaffected by either change of temperature or capping agent. Water-solubility of bio-functionalized CuS, ZnS and FeS nanoparticles was investigated. Amongst the three capping agents used, L-alanine (Ala) was found to be the most effective capping agent to render solubility of the nanoparticles. As the temperature was increased, the solubility of the particles also increased. Cytotoxicity

and antimicrobial activity of L-alanine-capped CuS and ZnS nanoparticles were investigated. The particles were less toxic at low to moderate concentrations and only induced toxicity at higher concentrations. Particles synthesized at 95 °C were less toxic compared to other nanoparticles (35 and 65 °C) for both two set of experiments, as informed by the CC_{50} values. Antimicrobial properties were tested using different strains of both positive and negative bacteria and fungi. It was found that Ala-capped CuS nanoparticles were more effective against the bacteria than Ala-capped ZnS nanoparticles.

TABLE OF CONTENTS

LIST OF ABRIATIONS

Ala	L-Alanine
Asp	L-Aspartic acid
a.u	Arbitrary units
CFCs	Chlorofluorocarbons
DDTC	Diethyldithiocarbamate
DNA	Deoxyribonucleic acid
Eg	Band gap energy
Fig	Figure
FTIR	Fourier transform infrared spectroscopy
HDA	Hexadecylamine
ICDD	International Centre for Diffraction Data
IR	Infra-red
JCPDS	Joint Committee on Powder Diffraction Standards
NIR	Near infrared region
nm	Nanometer
PL	Photoluminescence spectroscopy
QDs	Quantum dots
TAA	Thioacetamide

TEM	Transmission electron microscopy
TODAB	Trioctadecylmethylammonium bromide
TOPO	Tri-n-octylphosphine oxide
TOP	Tri-n-octylphosphine
SPIONs	Superparamagnetic iron oxide nanoparticles
UV	Ultra-violet
UV-Vis	Ultra-violet visible spectroscopy
XRD	X-ray diffraction spectroscopy

LIST OF TABLES

LIST OF FIGURES AND SCHEMES

Chapter 1

Introduction and literature review

---

1. Introduction

The word nanotechnology can be defined in a number of ways. In general, however, it is the manipulation and manufacturing of matter at the scale of 1–100 nm (Albrecht *et al*. 2006). In the nanoscale (1–100 nm), materials have unique properties that are different from those of the isolated atom and bulk materials. These properties depend largely on the size of the particles from which the material is made.

Nanotechnology is an interdisciplinary field which has arisen from different scientific disciplines. It is known to involve chemistry, physics, biology, engineering, and in recent times toxicology (Zhang 2003). Even with a large unproven track record in the environmental arena, nanotechnology offers great promise for delivering new and improved environmental technologies (Albrecht *et al*. 2006).

However, the production of nanomaterials could also lead to new environmental problems, such as new classes of toxins and environmental pollution (Zhang 2003). Control measures should be taken to ensure that nanotechnology does not create future problems, as has been the case for many technologies of the twentieth century, for example, the dramatic reduction in ozone in the upper atmosphere by chlorofluorocarbons (CFCs) which come from industrial solvents and military aircraft (Albrecht *et al*. 2006). Thus, much of the recent research efforts have been on developing new strategies to fabricate nanomaterials using biomolecules.

Amino acids and carbohydrates were used as capping ligands because of their potential applications in the design and development of nanoscale devices which has been recognized

as a green and efficient way for further exploitation as nanosensors for biomedical applications (Lee *et al*. 2009; Kim *et al*. 2005; Barrientos 2003).

Bio-functionalised nanomaterials could be produced using different methods, which results in different structures of nanomaterials. The basic structures of nanomaterials include nanoparticles, quantum dots (QDs), nanolayers, and nanotubes to name a few. These nanostructures are different in how they are made and how their atoms or molecules are ordered. Nanoparticles, which are a collection of tens to thousands of atoms measuring about 1–100 nm in aggregate diameter, are the most basic structure in nanotechnology (Zhang 2003).

These kind of nanoparticles are created atom by atom, so that the size and shape, of particles can be controlled by varying experimental conditions. For the past two decades, one of the areas of nanotechnology that has been most studied is the study of semiconductor nanoparticles or quantum dots due to their unique size-dependent optical and electrical properties (Liu *et al*. 2013; Duan *et al*. 2011; Nelwamondo *et al*. 2012).

1.1 Semiconductor nanoparticles

Semiconductor nanoparticles which are defined as particles with at least one dimension ranging from 1-20 nm have gained attention due to their promising applications. Due to extremely small size and high surface to volume ratio, the physicochemical properties of semiconductor nanoparticles-containing materials are quite different to those of the bulk materials as a result of quantum confinement effects (El-sayed 2001). Quantum confinement effects occur when the radius of the nanocrystals is below the exciton Bohr radius, which is described as the smallest possible radius of an electron orbiting the nucleus in an atom (Zhang *et al*. 2014).

In essence, when the size of the crystals decreases below the exciton Bohr's radius of the bulk material, the energy levels possess atom-like properties which become discrete as compared to the continuum energy levels observed in bulk materials (Singh *et al*. 2015). Thus, besides their unique physicochemical properties (small size and high reactivity), semiconductor nanoparticles act as a bridge between bulk materials and atomic or molecular structures, due to their better performance in applications. Therefore, they are a good candidate for applications including medical, catalysis, electrochemistry, biotechnology and trace-substance detection (Luo *et al*. 2006; Murthy 2007; Wen *et al*. 2011; Xia *et al*. 2013).

Various sizes of semiconductor nanoparticles with new properties have been synthesized using different methods and found to be interesting in many applications such as in biology (Salata 2004), optical sensors (Pereiro *et al*. 2006) and photovoltaics (Gawande *et al*. 2015). Looking at high drug resistance in the field of medicine, cellular imaging using semiconductor nanocrystals is advantageous, since they can emit light at a variety of wavelengths from ultraviolet to infrared just by varying their size and shape. The broad absorption and narrow emission spectra of semiconductor nanocrystals makes them well suited to multiplexed imaging, in which multiple colors and intensities are combined to encode genes, proteins and small molecule libraries (Yu *et al*. 2006; Talwatkar *et al*. 2014; Barroso 2011).

These developments in semiconductor nanocrystals research represent significant progress towards the generation of novel intracellular fluorescent probes for biological imaging of living cells and tissues (Law *et al*. 2009; Smith & Nie 2009). However for nanocrystals to be used for biological applications, they should meet a number of requirements, which include good water solubility, absorption in the near infrared region and have low toxicity. Most semiconductor nanocrystals are made from toxic materials, and therefore have limited prospects for future *in vivo* medical applications (Rao *et al*. 2002).

Synthesis of semiconductor nanocrystals using UV irradiation (Chili *et al*. 2012), aerosol (Didenko & Suslick 2005), hydrothermal (Aneesh *et al*. 2007) , sol-gel (Dawnay *et al*. 1997) and emulsion (Zielinska *et al*. 2011) methods to name a few, have resulted in small and well defined nanoparticles. However, these methods involve the use of organic solvents, hydrophobic capping agents, high temperature (>150 °C) and toxic reducing agents that generate an environmental risk (Khudhayer *et al*. 2012). Thus, a key understanding of improved synthesis processes is required which can use environmentally benign (less toxic, low temperature and cheap) materials and be able to be exploited at the industrial and commercial level to have better manufactured, long lasting, cleaner and safer products such as home appliances, communication technology, medicines and agriculture (Sharma *et al*. 2015). Therefore, the main focus recently in nanochemistry is to design nanoparticles using environmentally benign approaches. These provide solutions to growing challenges related to environmental issues.

Semiconductor nanocrystals are useful materials in the implementation of new technologies in the 21st century. They generally composed of atoms of groups II-VI, III-V or I-VI. In their synthesis, ligands such as hexadecylamine (HDA), trioctadecylmethylammonium bromide (TODAB), trioctylphosphine oxide (TOPO) and trioctylphosphine (TOP) have commonly been employed for capping purposes (Malik *et al*. 2002; Mao *et al*. 2014; Nyamen *et al*. 2014). The above ligands make the synthesized nanoparticles soluble in organic solvents such as toluene and chloroform (Burda *et al*. 2005; Sato *et al*. 2008). In the past decades, much work on semiconductor nanoparticles using different metals such as Cu, Zn, Fe, and chalcogenides such as S, Se, Te has been reported. Below is an exploration of some examples of semiconductor nanoparticles:

1.2 Copper sulphide (Cu_xS_y), zinc sulphide (ZnS) and iron sulphide (Fe_xS_y) nanoparticles

(a) Cu_xS_y nanoparticles

Copper sulfide is a material composed of elements of group IB and VIA. The material is well known for its electrical and magnetic properties which have been mainly explored for energy, catalysis, and biological related applications (Goel *et al*. 2014). It has also been reported to be very attractive for biological application among the chalcogenides semiconductor nanomaterials, since copper is less toxic and has antimicrobial activity (Nelwamondo *et al*. 2012). In comparison to cadmium-based semiconductors, copper based nanomaterials such as chalcocite (Cu_2S) are preferred since copper is a less toxic metal (Quintana-ramirez *et al*. 2014; Nelwamondo *et al*. 2012).

Copper sulfide is a p-type semiconductor with a direct band gap of 1.2 eV-2.0 eV (Ramasamy *et al*. 2013). This material is one of the most complicated metal sulfide, which has a number of phases and chemical compositions. It is known to have at least fourteen different identifiable phases (Ramasamy *et al*. 2013). Some of those identified phases include chalcocite (Cu_2S), djurleite ($Cu_{31}S_{16}$ or $Cu_{1:94}S$), digenite (Cu_9S_5 or $Cu_{1:8}S$), anilite (Cu_7S_4 or $Cu_{1:75}S$), covellite (CuS), and villamaninite (CuS_2) (Saeed *et al*. 2013).

For the past two decades, synthesis of copper sulfide nanoparticles has seen significant progress. Several methods such as microwave irradiation techniques, solid state reaction and colloidal synthesis have yielded nanoparticles with various shapes and that exhibit different properties (Bajpai *et al*. 2014;Tadjarodi & Khaledi 2010; Dutta & Dolui 2008). However, these synthetic methods result in hydrophobic nanoparticles. Larsen and co-workers reported a solvent less approach to synthesize copper sulfide nanorods from a thiolate-derived precursor by thermolysis. The nanorods obtained at 148 °C were 4 nm in diameter and 12 nm in length (Larsen *et al*. 2003). In situ source template interface reaction, a wet chemical

method was used to synthesize one-dimensional CuS twinned nanorods at a low temperature of 105 °C as a variation to the common solvothermal attempts (Roy *et al*. 2008).

(b) ZnS nanoparticles

The most popular semiconductor nanoparticles are those composed of group II-VI elements. Some examples of group II-VI compounds are CdS, ZnS, ZnSe, and CdSe, and they have shown to be important materials for the applications in optoelectronic devices (Ramasamy *et al*. 2013). ZnS with wide band gap energy of 3.7 eV is an important member of this family and has been extensively investigated as it has numerous applications to its credit (Soltani *et al*. 2012). For an example, it has been used widely as an important phosphor for photoluminescence, electroluminescence and cathodoluminescent devices due to its better chemical stability compared to other chalcogenides such as ZnSe (Rahdar 2013).

The synthesis of ZnS remains a topic of interest for researchers, as new synthetic routes are being explored to get a single phase material *via* an economically and technically suitable method. However, most of the synthetic routes yield low-quality nanoparticles having large size distribution. To obtain nanometre-sized particles, a variety of methods such as precipitation in aqueous and organic media (Borah *et al*. 2008), thermal decomposition (Yitai *et al*. 1995) and hydrothermal synthesis (Dumbrava *et al*. 2005) have been proposed. Yitai, *et al*. (Yitai *et al*. 1995) successfully prepared pure nanocrystalline ZnS phase (sphalerite) from amorphous ZnS, which was the natural precipitate of the reaction of $Zn(CH_3COO)_2$ and Na_2S. Dumbrava and co-worker successfully synthesized ZnS nanoparticles in a simple aqueous system, in the presence of surfactants, using $Zn(CH_3COO)_2$ and thiourea as the initial materials. The obtained nanoparticles were plane, and almost hexagonal in shape. The presence and nature of surfactant changed the morphology, particle size, and distribution of the final product (Dumbrava *et al*. 2005). Photophysical properties of ZnS nanoclusters have been studied by Kumbhojkar and co-

worker and the quantum size effect was clearly observed. They reported a significant effect of capping agents on optical properties demonstrated through variations of the emission peak energies of ZnS nanoclusters with a different capping agent (Kumbhojkar *et al*. 2000).

(c) Fe_xS_y nanoparticles

Iron sulfide exists in various and valuable stoichiometric compositions which are FeS_2, Fe_2S_3, Fe_3S_4, Fe_7S_8, and $Fe_{1-x}S$, FeS and $Fe_{1+x}S$ (Ramasamy *et al*. 2013). Among them, FeS_2 is a nonmagnetic semiconductor with an optical band gap of 0.9 eV (Vaughan 1978). In recent years there has been a considerable interest in the synthesis of nanocrystals of different composition of iron sulfide.

Numerous methods have yielded nanoparticles with various shapes exhibiting different properties (Ramasamy *et al*. 2013). Nath and co-workers successfully synthesized Fe_7S_8 nanowires in a solvothermal experiment using $FeCl_2.4H_2O$, thioacetamide, and ethylenediamine in Teflon-lined stainless steel autoclave for four days at 180 °C. The obtained nanowires had sizes that range from 80-100 nm in diameter (Nath *et al*. 2003). Vanitha and O'Brien, (Vanitha & O'Brien 2008) synthesized pyrrhotite type Fe_7S_8 and greigite type Fe_3S_4 nanoparticles from $[NnBu_4]_2[Fe_4S_4(SPh)_4]$ as single source precursor by varying solvent. Interestingly, the precursors yielded pyrrhotite Fe_7S_8 nanocrystals in octylamine at 180 °C but greigite Fe_3S_4 nanocrystals in dodecylamine at 200 °C. Both as-synthesized nanocrystals were spherical in shape with average sizes of 5.6 nm (pyrrhotite) and 3.5 nm (greigite) and both were super paramagnetic (Vanitha & O'Brien 2008).

Even though researchers have successfully done so much in the field of nanochemistry, efforts are still needed throughout the world to develop ecofriendly technologies to produce environmentally benign, nontoxic products using green nanotechnology and biotechnological tools. In addition degradation and accumulation studies are need also need to be considered. However in this study, we will explore the synthesis of nanoparticles using

green capping agents and less toxic metals like Cu, Zn and Fe which are found in the human biological system in trace amounts. The reason for this is to try to reduce the environmental impact of nanoparticles and to improve the biological application of nanoparticles.

1.3 Conditions affecting the properties of metal chalcogenide nanoparticles

The quality of semiconductor nanoparticles influences their properties and hence their potential applications. Efforts to control the synthesized nanoparticles are through many explorations of parameters, which then play a critical role in their properties and therefore potential applications. The parameters affecting the synthesis of nanoparticles includes temperature, time, precursor concentration and solvent, to name a few. Defect-free, well dispersed and homogeneous nanoparticles are highly desired for different applications. However optimizing each of these parameters to obtain ideal particles may be complex and practically difficult (Zhong *et al*. 2003).

The synthesis of nanoparticles involves the growth and nucleation of particles from their precursors heated in a coordinating solvent (Gebauer 2008). This is carefully monitored by investigating the temperature for a given synthesis (Gou & Murphy 2004). The Ostwald ripening effect is the main feature to be overcome when optimizing the temperature for synthesis of nanoparticles. This ripening effect allows particles to group together with smaller ones tending to deposit onto big ones to form larger particles (Ham *et al*. 2014). Li and co-wokers reported the synthesis of microsphere of covellite CuS at 90 °C and 120 °C for 24 h while increasing the temperature at the constant synthesis time reduced some of the CuS into digenite phase as Cu_9S_5 nanorods (Li *et al*. 2010). In another study Vidyasagar and co-wokers reported the synthesis of CuO nanoparticles at 400 and 800 °C and found that the intensity of peaks increased with increasing annealing temperature, as well as the optical band gap edge shifted towards longer wavelength region which was attributed to the

decreasing band gap of the CuO nanoparticles at higher temperatures (Vidyasagar *et al*. 2012).

1.4 General synthetic routes of semiconductor nanoparticles

Various methods have been developed for the preparation of semiconductor nanoparticles, some of those methods are colloidal, hydrothermal and single-molecule precursors. Below is a brief description of the above-mentioned methods:

1.4.1 Colloidal method

Colloidal semiconductor nanoparticles are synthesized from precursor compounds dissolved in solutions, much like traditional chemical processes. The synthesis of colloidal semiconductor nanoparticles is based on a three-component system composed of a precursor, organic surfactant, and solvent. The kinetics of nucleation and particle growth in homogenous solution can be adjusted by the controlled release of anions and cations (Laguna *et al*. 2016). Nanocrystals are commonly achieved by carrying out a precipitation reaction in a homogenous solution in the presence of stabilizers, which are used to prevent agglomeration and further growth of nanoparticles (Scher *et al*. 2003). La Mer and co-workers reported the synthesis of highly monodispersed micrometric colloids in which it was explained by means of nucleation and growth that are properly controlled (La Mer *et al*. 1994). In this method particles with dimensions of the order of nanometres can also be reproduced. Small crystals, which are less stable usually group together, and re-crystallize to form large and more stable crystals, this process is referred to as Ostwald ripening.

For the colloidal method to produce uniform particles, semiconductor nanoparticles must have low solubility, which can be achieved by correct choice of solvent, pH, temperature and a passivating agent. Highly monodispersed samples are obtained if nucleation and growth process are distinctly separated from one another. The colloidal growth stability of

the crystal can be improved by using solvents with low dielectric constants or by using stabilizers such as styrene/maleic acid copolymer (Samoilova *et al*. 2009). One of the first attempts to produce group II-VI semiconductor by Spenhel and co-workers was the synthesis of the colloidal suspensions where CdS was formed by reacting H_2S with cadmium salt in aqueous solution (Spanhel *et al*. 1987).

Extensive research has been done in the synthesis and characterization of colloidal group II-VI semiconductor nanoparticles (Rogach *et al*. 1999). In the past decade, various surfactants, organic or inorganic polymers, thiols, amines and polyphosphates (Oluwafemi & Songca 2006; Sondi *et al*. 2004; Nanda *et al*. 2000; Roy & Srivastava 2007) have been used and reported in the literature to be good stabilizing agents for the as-synthesized colloidal semiconductor nanoparticles. The specific adsorption of surfactants to the individual crystallographic planes changes the relative growth rates of different facets, providing a way of controlling the nanocrystal shape.

Recently, there have been many studies on the solution-phase preparation of semiconductor nanoparticles stabilized by various surfactants at low temperatures (Law *et al*. 2009; Ajibade & Mbese 2014; Bansal *et al*. 2012). Kruszynska and co-workers have successfully synthesized CuS nanorods by colloidal method aided with various nucleation temperature and copper monomer concentration. By adjusting the nucleation temperature and copper monomer concentration, control over the length of the CuS nanorods was achieved (Kruszynska *et al*. 2012). This compliment the fact that reaction parameters play an important role in the control of nanoparticles shape and sizes. More recently Augustine and co-workers successfully synthesized bio-compatible ZnS:Mn nanocrystals using chitosan and amino acid ligands as capping materials. The method employed requires no complex procedure, applies low temperature and green capping molecules (Augustine *et al*. 2015). These makes the method be a relatively green chemical alternative.

The colloidal method is regarded as one of the good methods used in the preparation of nanosized semiconductor particles. The advantage of employing this method is that large batches of quantum dots may be synthesized, and it is acknowledged as one of the least toxic routes for the synthesis of quantum dots, due to use of low temperatures and green capping molecules. However, some shortcomings of this method are that it could not be employed to easily synthesize some types of semiconductors like CdSe, GaAs, InP, and InAs and the instability of particles being produced at high temperatures, makes annealing of the particles difficult, which leads to poor crystalline materials being formed (Shumbula 2011).

1.4.2 **Hydrothermal method**

Hydrothermal synthesis is a common method used to synthesize zeolite/molecular sieve crystals. This method manipulates the solubility of almost all inorganic substances dissolved in water at elevated temperatures and pressures, and subsequent crystallization of the dissolved material from the solution (Bhushan *et al.* 2014). At elevated temperatures, water plays an important role in the transformation of the precursor because the vapor pressure is much higher and the phase of water at elevated temperatures is different from that of room temperature. The properties of the reactants, including their solubility and reactivity, also change at high temperatures. The changes enable the fabrication of high-quality nanoparticles which is not possible at low temperatures. Parameters such as pressure, temperature, reaction time, concentration and precursors can be tuned to maintain a high simultaneous nucleation rate and good size distribution (Liu *et al*. 2013). Different types of nanoparticles such as CuS, ZnS/ZnO, and FeS_2 have been successfully synthesized employing a hydrothermal method (Saranya & Nirmala Grace 2012; Kanti Kole *et al*. 2014; Liang *et al*. 2016). However, the disadvantages of this method are that high temperature and long synthesis hours are usually required. In addition, the solvent is not limited to water but

also includes other polar or nonpolar solvents, such as benzene and the process is more appropriately called a solvothermal synthesis.

1.4.3 **Single-molecule precursors**

The challenges associated with the use of toxic and volatile compounds such as metal alkyls at elevated temperatures led to the development of alternative chemical routes to nanoparticles. One of the approaches to overcoming this challenge is the use of single molecular precursors, i.e. a single compound containing all elements required within the nanocrystallite, such as alkyldiseleno or alkyldithiocarbamato complexes. O'Brien's and co-authors has studied the decomposition of various single molecular precursors (Revaprasadu *et al*. 1999; Oluwafemi *et al*. 2008; Malik *et al*. 2001; Sreekumari Nair *et al*. 2003) and the effect of different organic ligands such as TOPO, octylamine (Wang *et al*. 2006) and haxadecylamine (Malik *et al*. 2004) in the synthesis of CuS, ZnO, ZnSe nanoparticles (Malik *et al*. 1999; Nyamen *et al*. 2014).

Sun, *et al*. (Sun *et al*. 2008) reported the synthesis of hexagonal phase ZnS nanoparticles by microwave thermolysis of a single-source molecular precursor of zinc diethyldithiocarbamate ($Zn(DDTC)_2$) in ethylene glycol at 110 ^{o}C for 5 min. The average size obtained was 5 nm, and this was surprising since the method was able to achieve a high-temperature stable phase at very low temperature. Thus, this method provides economically viable route for applications of nanopartilces but also opens a new avenue to study structural kinetics and chemistry of semiconductor nanoparticles. There are a number of potential advantages of using single-source/molecular precursors over other existing routes, such as (i) low-temperature deposition routes are possible, (ii) single source routes avoid the need for volatile, sometimes toxic and/or pyrophoric precursors. All precursor synthesis is carried out under anaerobic conditions, with the resulting precursors being air and moisture stable, (iii) although there are theoretical models predicting the optical properties of semiconductor

nanoparticles, the properties of nanoparticles obtained by new synthetic routes are sometimes hard to anticipate and may lead to particles with and unanticipated, but useful, properties (Trindade *et al*. 2001; Pickett & O'Brien 2001).

1.5 Green chemistry

The partial or total elimination of waste along with sustainable processes is known as green chemistry, which employs nontoxic chemical and renewable materials (Khudhayer *et al*. 2012). For the past few years, the 'green' environmentally friendly processes in chemistry and chemical technology are becoming increasingly popular and are much needed as a result of worldwide problems associated with environmental contamination. Green chemistry for the preparation of nanoparticles involves techniques that use naturally-occurring reagents such as vitamins, amino acids, sugars, plant extracts, biodegradable polymers, and microorganisms as reducing and capping agents (Kharissova *et al*. 2013). In the past two years, several 'green chemistry' books have been published describing green processes for the synthesis of nanoparticles and their specialized aspects, including ultrasound, microwaves, and other methods (Anastas & Li 2013; Manahan 2009).

1.5.1 Green capping agents: Types and properties

Capping agents play a very important and versatile role in the nanoparticles synthesis. Nanoparticles can be functionalized and stabilized using capping agents to impart useful properties by controlling morphology, size and protecting the surface thereby preventing agglomeration (Sharma *et al*. 2015). Many commonly used surfactants e.g. HDA have been reported to be used as capping agents for varying the desired shape and size of the nanoparticles but most are difficult to remove and do not easily degrade. Therefore, most of the commonly used surfactants are hazardous to the environment since they are not biodegradable (Gittins *et al*. 2000; Liu *et al.* 2005). In the view of the hazardous nature of

these chemicals, there is an urgent need to use environment-friendly capping agents and design green biochemical routes at the laboratory and industrial level for the synthesis of nanoparticles (Sharma *et al*. 2015). Surface functionalisation of nanoparticles plays an important role in bio-applications.

1.5.1.1 Amino acids capped nanoparticles

The preparation of nanoparticles in the same solvent using biomolecules has recently gained interest due to their non-toxic nature and not involving harsh synthetic procedures (Sharma *et al*. 2015). Beyond their inherent environmental advantages, their specific molecular properties provide the basis for precise control over the morphology of nanoparticles.

In the general context of nanoparticle synthesis, the adsorption of capping agents largely determines the morphologies of ultimate nanoparticles by affecting the reaction dynamics as well as the preferential growth in different directions. Thus, a controllable synthesis characterized by programmable products could only be realized when the adsorption ability of capping agent is adjustable (Duan *et al*. 2015). Proteins and peptides are composed of a wide selection of amino acids with distinct adsorption abilities of the precursors and nanoparticles, the versatility of which is further enhanced by the considerable possibilities of a sequence of the amino acids in the proteins or peptides (Duan *et al*. 2015). In this context, the synthetic process could be rationally controlled.

Nelwamondo and co-workers successfully synthesized water-soluble CuS nanoparticles with a single crystal phase using alanine as the stabilizing ligand. The highest synthetic temperature (100 °C) resulted in particles with properties superior to the ones synthesized at lower temperatures (40 and 70 °C) and the surface coverage of the nanoparticles with alanine improved with increasing temperature evident from the degree of water solubility of the particles (Nelwamondo *et al*. 2012).

In another study, CdS nanoparticles with good optical properties were successfully synthesized using three different amino acids (serine, alanine, and histidine) as the stabilizing agents by one-pot synthesis method with low toxic properties (Samadi-maybodi *et al*. 2014). The CdS nanoparticles showed good photocatalytic activities to degrade the organic dyes (alizarin) under visible light irradiation, suggesting its potential application in the effective treatment of the organic pollutants under visible light irradiation. In addition, a decrease in the photocatalytic efficiency of the synthesized nanoparticles was observed on the degradation of alizarin with an increase in their size; thus follows the order L-serine > L-histidine > D-alanine. Heo and Hwang successfully synthesized L-Aspartic acid-capped ZnS:Mn nanocrystals. The prepared water-dispersible L-Asp-capped ZnS:Mn nanocrystals showed physicochemical properties for applications in an advanced photosensor device. The nanoparticles were used as a photosensor for the detection of specific cations in aqueous solution (Heo & Hwang 2016).

On another study by Farahnak and Nematollah (Farahnak & Nematollah 2014) spherical Au nanoparticles were synthesized using aspartic acid, glutamic acid, and tryptophan as reducing agents. Particles produced using glutamic acid were found to be larger on average than those produced under identical conditions using aspartic acid while the particles produced by tryptophan had the largest size (Farahnak & Nematollah 2014). Through direct utilization of small biomolecules as the capping agents, synthesis of the nanoparticles could be simplified, yielding bio-functionalized catalysts as compared with current state of the art catalyst.

1.5.1.2 Disaccharides

The biocompatibility and specific receptor recognition ability make carbohydrates as potential targeting ligands to modify nanoparticles for site-specific bio applications. Carbohydrates not only enable specific targeting, but they also grant water solubility and

biocompatibility as well to the nanoparticles, which is necessary for their safe use in bio-based applications (Watson 2015). Disaccharides, meaning "two sugars," are a class of polymeric carbohydrate molecules with repeating units of monosaccharides linked together by glycosidic linkages. They act as capping agents in the synthesis of nanoparticles as they are hydrophilic, stable, safe, low at cost, biodegradable and non-toxic. The synthesis is normally carried out in the presence of water as a solvent, thus eliminating the use of toxic solvents (Akhlaghi *et al*. 2013; Duan *et al*. 2015).

Carbohydrate functionalization on nanoparticles surfaces happens in one of two ways, either the carbohydrate ligand is synthesized at first and later functionalized to the surface, or the carbohydrate is attached to the surface through some bioconjugation method. Tamura and co-worker synthesized a hydrophilic phosphine oxide linked with mannose moieties *via* the amide linkage and synthesized CdSe–ZnS quantum dots *via* the ligands surface addition instead of TOPO (Tamura *et al*. 2002). Sun and co-workers reported the synthesis of branched glycopolymer, displaying galactose–glucose disaccharides, with a biotinylated end group attached to streptavidin-coated CdSe–ZnS quantum dots and successfully showed the capture and detection of nanomolar lectin (Sun *et al*. 2004).

In another study, Ahire and co-workers synthesized silicon nanoparticles (SiNPs) capped with carbohydrates including galactose, glucose, mannose, and lactose from amine terminated silicon nanoparticles (Ahire *et al*. 2015). The MTT [3-(4, 5-dimethylthiazol-2-yl)-2, 5-diphenyltetrazolium bromide] analysis showed an extensive reduction in toxicity of silicon nanoparticles by functionalizing with carbohydrate moiety both *in vitro* and *in vivo* studies. Thus, disaccharides are one of the renewable green alternatives for the fabrication of nanoparticles replacing toxic chemicals thereby saving the environment from their hazardous effects.

1.6 Water solubility of semiconductor nanoparticles/quantum dots

Semiconductor nanoparticles are of interest because of their photo-physical properties. The surface plays a vital role in both the physical and chemical properties of these nanoparticles. The nature of the surface can be influenced by many aspects including solubility, reactivity, stability and electronic structure (Alivisatos 1996). One of the challenges for using semiconductor nanoparticles in biological studies is to design hydrophilic, yet highly luminescent, semiconductor nanoparticles with a surface that is adaptable to varied biological applications. Synthesis of semiconductor nanoparticles using high boiling points solvents is commonly employed to produce high-quality nanoparticles, but there has been interest in developing water-soluble nanoparticles with comparable quality. The water solubility can be increased by adding capping agents with two functional groups, one group should have an affinity for the semiconductor nanoparticles surface (e.g., thiol, carbonyl, hydroxyl or amine) and the other must be a polar group (e.g., carboxylate) to make the nanoparticles soluble in aqueous media. There are a number of methods used to impart water solubility of nanoparticles, such as silica encapsulation, ligand exchange, and hydrophobic interaction. However the above methods still possess some disadvantages, e.g., ligands exchange method alters the chemical and physical properties of semiconductor nanoparticles which result in a decrease in the quantum yield (Kim *et al*. 2005). Therefore to solve some of these challenges, scientists have embarked on preparing nanoparticles directly in aqueous solution.

1.7 Cytotoxicity of semiconductor nanoparticles

Considerations of semiconductor nanoparticles cytotoxicity can be challenging due to variety of semiconductor nanoparticles being synthesized. In order to clarify or simplify this topic, it should be emphasized that not all semiconductor nanoparticles are similar. Each individual type of semiconductor nanoparticles possesses its own unique physicochemical

properties, which in turn determines its potential cytotoxicity. Semiconductor nanoparticles contain toxic components, such as cadmium (from cadmium chalcogenide-based quantum dots) or lead (from lead chalcogenide-based quantum dots). Cd^{2+} and Pb^{2+} could be released from quantum dots and then kill the mammalian cells (Fischer & Skreb 2001).

The extent of cytotoxicity has been found to be dependent upon a number of factors such as size, coating agents, colour, a dose of quantum dots, mechanical stability, photolytic, oxidative, surface chemistry, coating bioactivity and processing parameters (Shiohara *et al*. 2004; Hardman 2006). Some semiconductor nanoparticles like cadmium-containing semiconductor nanoparticles have been found to be cytotoxic only after oxidative and/or photolytic degradation of their core coatings (Jin *et al*. 2011). However, it must be noted that studies that are specifically designed for toxicological assessment are very few. In this way, a direct way to avoid the possible toxicity of quantum dots is to make them well coated to become biologically inert. The coating materials can be low or nontoxic organic molecules or polymers (e.g. polyethylene glycol) or inorganic layers (e.g. ZnS and silica) (Yu *et al*. 2006).

1.8 Application of nanotechnology

The benefits derived from nanotechnology depend on the fact that it is possible to tailor the essential structures of materials at the nanoscale to achieve specific properties. Nanotechnology is used in many computing, communications, and other electronics applications to provide faster, smaller, and more portable systems that can manage and store larger amounts of information. Some of the nanoparticles synthesized in this present study have found applications in biological uses.

1.8.1 Biomedical application of nanoparticles

The biological and medical research communities have exploited the unique properties of nanomaterials for various applications. Semiconductor nanoparticles have been reported to

have a wide array of potential biomedical applications, especially when combined with antigen- specific coatings or functional groups on their surfaces (Li *et al*. 2016). The advances in synthesis and functionalization of nanoparticles have brought a significant increase in their biomedical applications, including imaging of cell and tissues, drug delivery, sensing of target molecules, and much more. Below are some of the common applications of nanoparticles in biomedical systems.

(a) Cellular labelling

One of the most important uses of fluorescent probes in biology is the labeling of cellular structures (Jensen 2012). Naturally, the earliest demonstrated uses of quantum dots (QDs) in biology were to label cells with a new class of bright and stable fluorophores (Mattoussi & Clapp 2008). Multicolour labeling of cells is a powerful technique for visualizing many of these structures simultaneously, such as cytoskeletal proteins or organelles, and to elucidate intracellular processes (Brandenburg & Zhuang 2009). Although cell labeling with organic dyes has been popular for past decades, the use of multiple labels simultaneously remains a cumbersome procedure due to the narrow absorption profiles of most dyes (Mattoussi & Clapp 2008). Effective multicolour labelling requires an assortment of filters to properly excite and collect fluorescence from specific dye molecules. The continuous excitation of dyes inevitably results in significant photo-bleaching that quenches the luminescence over short time scales. This severely limits the practical observation time for sample, even with the addition of various anti-bleaching chemical agents (Lakowicz 2006).

By contrast, QDs are excellent fluorescent probes for long-term multicolour cell labelling. They have been widely used as luminescent cell markers that identify molecular structures. However, overcoming the challenge of creating stable, water soluble materials that could be delivered within cells is difficult. However, with the availability of commercial labelling kits, the prevalence of QDs in cell labelling applications has increased dramatically.

Regardless of their popularity and success, commercial materials currently have somewhat limited potential due to the use of specific proprietary coatings and surface ligands to passivate and stabilize the nanoparticles (Shumbula 2011).

(b) Antimicrobial activity

An antimicrobial refers to a substance that kills or inhibits the growth of microorganisms. Since the discovery of antimicrobial drugs in the 1960s (Coates *et al*. 2002), many infectious diseases have been overcome. Typically, antimicrobials kill bacteria by binding to some vital compounds of bacterial metabolism, thereby inhibiting the synthesis of functional biomolecules or impeding normal cellular activities. For instance, lactams such as penicillins and cephalosporins inhibit bacteria cell wall synthesis (Zeng & Lin 2013); tetracyclines, macrolides, and clindamycin inhibit protein synthesis (Beckers *et al*. 1995); metronidazole and quinolones inhibit nucleic acid synthesis; and sulphonamides and trimethoprim have an inhibitory effect on enzyme synthesis (Zhang *et al*. 2010). Some antimicrobials such as penicillin are only effective against a narrow range of bacteria, whereas others, like ampicillin, kill a broad spectrum of Gram-positive and Gram-negative bacteria (Walker 2000). Despite the great progress in antimicrobial development, many infectious diseases, especially intracellular infections, remain difficult to treat. One major reason is that many antimicrobials are difficult to transport through cell membranes and have low activity inside the cells, thereby imposing negligible inhibitory or bactericidal effects on the intracellular bacteria. In addition, antimicrobial toxicity to healthy tissues poses a significant limitation to their use (Stoyanova *et al*. 2016).

Over the last few decades, the applications of nanotechnology in medicine have been extensively explored in many medical areas, especially in drug delivery. By loading drugs into nanoparticles through physical encapsulation, adsorption, or chemical conjugation, the pharmacokinetics and therapeutic index of the drugs can be significantly improved in

contrast to the free drug counterparts (Zhang *et al*. 2010). Many advantages of nanoparticle based drug delivery, such as improvement of serum solubility of the drugs, prolonging the systemic circulation lifetime, releasing drugs at a sustained and controlled manner, preferentially delivering drugs to the tissues and cells of interest, and concurrently delivering multiple therapeutic agents to the same cells for combination therapy have been recognized (Zhang *et al*. 2008; Davis *et al*. 2008; Peer *et al*. 2007). Moreover, drug-loaded nanoparticles can enter host cells through endocytosis and then release drug payloads to treat microbes induced intracellular infections. As a result, a number of nanoparticle based drug delivery systems have been approved for clinical uses to treat a variety of diseases and many other therapeutic nanoparticle formulations are currently under various stages of clinical tests (Zhang *et al*. 2008; Wagner *et al*. 2006).

(c) Nanoparticles for pathogen detection and separation

Various nanoparticles platforms have been explored as sensors for detection and separation of pathogens (Wang & Wang 2015). Most strategies for pathogen detection have utilized optical and magnetic properties of nanoparticles platforms. One of the most common methods used for the detection of bacteria has been through the use of magnetic biosensors that involves direct immunological reactions using magnetic nanoparticles coated with antibodies against surface antigens (Varshney & Li 2007; Xia *et al*. 2006). Xai and co-workers applied this immunomagnetic approach in a novel microfluidic device to attract molecules bound to magnetic nanoparticles from one laminar flow path to another via a local magnetic field gradient (Xia *et al*. 2006). Using this device, *E. coli* label with biotinylated *anti-E.coli* antibody and bound to streptavidin-coated superparamagnetic iron oxide nanoparticles (SPIONs) were efficiently separated from solutions containing densities of red blood cells similar to blood.

Optical biosensing of bacteria has also been employed using metallic nanoparticles. The bio-barcode assay approach (Nam *et al*.1884) provides amplification and the possibility of simultaneously detecting many different targets in one sample. Using this method, *Bacillus subtilis* double stranded genomic DNA was detected at a 2.5 frequency-modulated (fM) concentration (Hill *et al*. 2007). Similarly, *Salmonella enteritidis* was detected a 0.2 fM (Zhang *et al*. 2009). Nanoparticles have also been used as pathogen sensors. Edgar *et al*. reported a technique that combined *in vivo* biotinylation of engineered host-specific bacteriophage and attachment of the phage to streptavidin-coated nanoparticles (Edgar *et al*. 2006). The method provides specific detection of *E. coli* among several different bacterial strains and can detect as few as 10 bacteria/mL of the experimental samples.

1.9 Project aim and objectives

The aim of the project was to synthesize and characterize water-soluble Cu_xS_y, ZnS and Fe_xS_y semiconductor nanoparticles using colloidal method and to evaluate the cytotoxicity of these nanomaterials using MTS assay. In order to fulfill the above-mentioned aim, the following objectives were identified:

- Synthesis of water-soluble Cu_xS_y, ZnS and Fe_xS_y nanoparticles with the use of different capping agents (L-alanine, L-aspartic acid, and β-lactose). This involves the use of copper(II) chloride, zinc chloride, and iron(II) chloride monohydrade, as metal sources, and thioacetamide (TAA) as the sulphur source.
- Characterization of the functional groups on water-soluble Cu_xS_y, ZnS and Fe_xS_y nanoparticles using Fourier transform infrared (FTIR) spectroscopy, optical properties of the nanoparticles using Ultraviolet-visible (UV-Vis) and Photoluminescence (PL) spectroscopy.

- Study the influence of temperature on size and morphological structure of water-soluble Cu_xS_y, ZnS and Fe_xS_y nanoparticles using Transmission electron microscopy (TEM) and X-ray diffraction (XRD) spectroscopy.
- Investigation of the cytotoxicity of the selected nanoparticles.

1.10 References

AHIRE, J.H., BEHRAY, M., WEBSTER, C.A., WANG, Q., SHERWOOD, V., SAENGKRIT, N., RUKTANONCHAI, U., WORAMONGKOLCHAI, N., and CHAO, Y., 2015. Synthesis of carbohydrate capped silicon nanoparticles and their reduced cytotoxicity, *in vivo* toxicity, and cellular uptake. *Advanced Healthcare Materials*, **4**,1877–1886.

AJIBADE, P.A., and MBESE, J.Z., 2014. Synthesis and characterization of metal sulfides nanoparticles/poly (methyl methacrylate) nanocomposites. *International Journal of Polymer Science*, **2014**, 1–9.

AKHLAGHI, S.P., PENG, B., YAO, Z., and TAM, K.C., 2013. Sustainable nanomaterials derived from polysaccharides and amphiphilic compounds. *Soft Matter*, **9**, 7905.

ALBRECHT, M.A., EVANS, C.W., and RASTON, C.L., 2006. Green chemistry and the health implications of nanoparticles. *Green chemistry*, **8**, 417–432.

ALIVISATOS, A.P., 1996. Perspectives on the physical chemistry of semiconductor nanocrystals. *Journal of Physical Chemistry.*, **100**, 13226–13239.

ANASTAS, P.T., and LI, C., 2013. *Handbook of Green Chemistry*: *Green Processes*, Weinheim: Wiley-VCH Verlag & Co. KGaA.

ANEESH, P.M., VANAJA, K.A., and JAYARAJ, M.K., 2007. Synthesis of ZnO nanoparticles by hydrothermal method. *Nanophotonic Materials IV*, **6639**, 1–9.

AUGUSTINE, M.S., ANAS, A., DAS, A.V., SREEKANTH, S., and JAYALEKSHMI, S., 2015. Cytotoxicity and cellular uptake of ZnS : Mn nanocrystals biofunctionalized with chitosan and aminoacids. *Spectrochimica Acta Part A: Molecular and Biomolecular Spectroscopy*, **136**, 327–333.

BAJPAI, P.K., YADAV, S., TIWARI, A., and VIRK, H.S., 2014. Recent advances in the synthesis and characterization of chalcogenide nanoparticles. *Solid State Phenomena*, **222**, 187–233.

BANSAL, P., JAGGI, N., and ROHILLA, S.K., 2012. "Green" Synthesis of CdS nanoparticles and effect of capping agent concentration on crystallite size. *Research Journal of Chemical Sciences*, **2**, 69–71.

BARRIENTOS, A.G., FUENTE, J.M., ROJAS, T.C., FERNANDEZ, A., and PENADES, S., 2003. Gold glyconanoparticles : Synthetic polyvalent ligands mimicking glycocalyx-like surfaces as tools for glycobiological studies. *Chemistry a European Journal*, **9**,1909–1921.

BARROSO, M.M., 2011. Quantum Dots in Cell Biology. *Journal of Histochemistry & Cytochemistry*, **59**, 237–251.

BECKERS, C.J.M., ROOS, D.S., DONALD, R.G.K., LUFT, B.J., SCHWAB, J.C., CAO.Y., and JOINER, K.A.,1995. Inhibition of cytoplasmic and organellar protein synthesis in toxoplasma gondil implications for the target of macrolide antibiotics. *Journal of Clinical Investigation*, **95**, 367–376.

BHUSHAN, B., LUO, D., SCHRICKER, S.R., SIGMUND, W., and ZAUSCHER, S., 2014. *Handbook of Nanomaterials Properties*, Springer-Verlag Berlin Heidelberg.

BORAH, J.P., BARMAN, J., and SARMA, K.C., 2008. Structural and optical properties of ZnS nanoparticles. *Chalcogenide Letters*, **5**, 201–208.

BRANDENBURG, B., and ZHUANG, X., 2009. Virus trafficking–learning from single-virus tracking. *Nature Reviews Microbiology*, **5**, 197–208.

BURDA, C. CHEN, X., NARAYANAN, R., and EL-SHAYED, M.A., 2005. Chemistry and

Properties of Nanocrystals of Different Shapes, *Chemical Reviews*, **105**, 1025–1101.

CHILI, M.M., PULLABHOTLA, V.S.R.R., and REVAPRASADU, N., 2012. Synthesis of PVP-capped Au-CdSe hybrid nanoparticles. *ISRN Metallurgy*, **2012**, 1–4.

COATES, A., HU, Y., BAX, R., and PAGE, C., 2002. The future challenges facing the development of new antimicrobial drugs. *Nature Reviews Drug Discovery*, **1**, 895–910.

COLVIN, V.L., SCHLAMP, M.C., and ALIVISATOS, A.P., 1994. Light-emitting-diodes made from cadmium selenide nanocrystals and a semiconducting polymer. *Nature*, **370**, 354–357.

DAVIS, M.E., CHEN, Z.G., and SHIN, D.M., 2008. Nanoparticle therapeutics : an emerging treatment modality for cancer. *Nature Reviews Drug Discovery*, **7**, 771–782.

DAWNAY, E.J.C., FARDAD, M.A., GREEN, M., and YEATMAN, E.M., 1997. Growth and characterization of semiconductor nanoparticles in porous sol-gel films. *Journal of Material Research*, **12**, 3115–3125.

DIDENKO, Y.T., and SUSLICK, K.S., 2005. Chemical aerosol flow synthesis of semiconductor nanoparticles. *Journal of American Chemical Society*, **127**, 12196–12197.

DUAN, H., WANG, D. and LI, Y., 2015. Green chemistry for nanoparticle synthesis. *Chemical Society reviews*, **44**, 5778–5792.

DUAN, J. JIANG, X., NI, S., YANG, M., and ZHAN, J., 2011. Talanta facile synthesis of N-acetyl-l-cysteine-capped ZnS quantum dots as an eco-friendly fluorescence sensor for Hg^{2+}. *Talanta*, **85**, 1738–1743.

DUMBRAVA, A., CIUPINA, V., and PRODAN, G., 2005. Dependence on grain size and morphology of zinc sulfide particles by the synthesis route. *Romanian Journal of Physics*, **50**, 831–836.

DUTTA, A., and DOLUI, S.K., 2008. Preparation of colloidal dispersion of CuS nanoparticles stabilized by SDS. *Materials Chemistry and Physics*, **112**, 448–452

EDGAR, R. MCKINSTRY, M., HWANG, J., OPPENHEIM, A.B., FEKETE, R.A., GIULIAN, G., NAGASHIMA, K., and ADHYA, S., 2006. High-sensitivity bacterial detection using biotin-tagged phage and quantum-dot nanocomplexes. *Applied Biological Sciences*, **103**, 4841–4845.

EL-SAYED, M.A., 2001. Some interesting properties of metals confined in time and nanometer space of different shapes. *Accounts of Chemical Research*, **34**, 257–264.

FARAHNAK, M.Z., NEMATOLLAH, Z., FARHANGI, A., and AKBARZADEH, A., 2014. Preparation and characterization of gold nanoparticles with amino acids, examination of their stability. *Indian Journal of Clinical Biochemistry*, **29**, 306–314.

FISCHER, A.B., and KREB, Y., 2001. *In vitro* toxicology of heavy metals using mammalian cells: an overview of collaborative research data. *Archives of Industrial Hygiene and Toxicology*, **50**, 333–354

GAWANDE, M.B., GOSWAMI, A., ASEFA, T., GUO, H., BIRADAR, A.V., PENG, D.L., ZBORIL, R., and VARMA, R., 2015. Core–shell nanoparticles: synthesis and applications in catalysis and electrocatalysis. *Chemical Society Reviews*, **44**, 56–58.

GEBAUER, D., VOLKEL, A., and COLFEN, H., 2008. Stable prenucleation calcium carbonate clusters. *Science*, **120**, 1819–1823.

GITTINS, D.I., BETHELL, D., SCHIFFRIN, D.J., and NICHOLS, R.J., 2000. A nanometre-

scale electronic switch consisting of a metal cluster and redox-addressable groups. *Nature*, **408**, 67–69.

GOU, L., and MURPHY, C.J., 2004. Controlling the size of Cu_2O nanocubes from 200 to 25 nm. *Journal of Materials Chemistry*, **14**, 735.

GOEL, S., CHEN, F. and CAI, W., 2014. Synthesis and biomedical applications of copper sulfide nanoparticles: from sensors to theranostics. *Small (Weinheim an der Bergstrasse, Germany)*, **10**, 631–645.

HAM, H., PARK, N.H., KIM, S.S., and KIM, H.W., 2014. Evidence of Ostwald ripening during evolution of micro-scale solid carbon spheres. *Scientific reports*, **4**, 3579.

HARDMAN, R., 2006. A toxicologic review of quantum dots: Toxicity depends on physicochemical and environmental factors. *Environmental Health Perspectives*, **114**, 165–172.

HEO, J., and HWANG, C., 2016. Application of L-aspartic acid-capped ZnS : Mn colloidal nanocrystals as a photosensor for the detection of copper (II) ions in aqueous solution. *Nanomaterials*, **6**, 82.

HILL, H.D., VEGA, R.A. and MIRKIN, C.A., 2007. Nonenzymatic detection of bacterial genomic DNA using the bio bar code assay DNA. These blockers bind to specific regions of the target rehybridizing, which allows the particle probes to bind. *Analytical Chemistry*, **79**, 9218–9223.

JENSEN, E.C., 2012. Use of fluorescent probes : Their effect on cell biology and limitations. *The Anatomical Record*, **295**, 2031–2036.

JIN, S., HU, Y., GU, Z., LIU, L., and WU, H.C., 2011. Application of quantum dots in biological imaging. *Journal of Nanomaterials*, **2011**, 1–13.

KANTI, K.A., SEKHAR, T.C., and KUMBHAKAR, P., 2014. Morphology controlled synthesis of wurtzite ZnS nanostructures through simple hydrothermal method and observation of white light emission from ZnO obtained by annealing the synthesized ZnS nanostructures. *Journal of Materials Chemistry C*, **2**, 4338.

KIM, B., HONG, D., BAE, J., and LEE, M., 2005. Controlled self-assembly of carbohydrate conjugate rod-coil amphiphiles for supramolecular multivalent ligands. *Journal of American Chemical Society*, **127**, 16333–16337.

KIM, S., ZIMMER, J.P., OHNISHI, S., TRACY, J.B., FRANGIONI, J.V., and BAWENDI, M.G., 2005. Engineering $InAs_x P_{1-x}$/ InP/ ZnSe III-V alloyed core/ shell quantum dots for the Near-Infrared. *Journal of American Chemical Society*, **127**, 10526–10532.

KRUSZYNSKA, M., BORCHERT, H., BACHMATIAK, A., RUMMELI, M.H., BUCHNER, B., PARISI, J., and KOLNY-OLESIAK, J., 2012. Size and shape control of colloidal copper (I) sulfide nanorods. *American Chemical Society Nano*, **6**, 5889–5896.

KUMBHOJKAR, N., NIKESH, V. V., KSHIRSAGAR, A., and MAHAMUNI, S. 2000. Photophysical properties of ZnS nanoclusters. *Journal ofApplied Physics*, **88**, 6260.

LAGUNA, M., NUÑEZ, N.O., RODRÍGUEZ, V., CANTELAR, E., STEPIEN, G., GARCÍA, M.L., FUENTE, J.M., and OCAÑA, M., 2016. Multifunctional Eu-doped $NaGd(MoO_4)_2$ nanoparticles functionalized with poly(L-lysine) for optical and MRI imaging. *Dalton Transactions*, **45**,16354–16365.

LAKOWICZ, J.R., 2006. *Principles of Fluorescence Spectroscopy Principles of Fluorescence Spectroscopy*. 3rd ed. Baltimore, Maryland, USA: Springer ,

LARSEN, T.H., SIGMAN, M., GHEZELBASH, A., DOTY, R.C., and KORGE, B.A., 2003.

Solventless synthesis of copper sulfide nanorods by thermolysis of a single source thiolate-derived precursor. *Journal of the American Chemical Society*, **125**, 5638–5639.

LAW, W.C., YONG, K.T., ROY, I., DING, H., HU, R., ZHAO, W., and PRASAD, P.N., 2009. Aqueous-phase synthesis of highly luminescent CdTe/ZnTe core/shell quantum dots optimized for targeted bioimaging. *Small*, **5**, 1302–1310.

LEE, S., KIM, K., and HWANG, C., 2009. Syntheses and characterizations of valine and alanine capped water soluble ZnS nanoparticles. *Journal of the Korean Chemical Society*, **53**, 505–511.

LI, F., WUA, J., QIN, Q., LI, Z., and HUANG, X., 2010. Controllable synthesis, optical and photocatalytic properties of CuS nanomaterials with hierarchical structures. *Powder Technology*, **198**, 267–274.

LI, X., WEI, J., AIFANTIS, K.E., FAN, Y., FENG, Q., CUI, F., and WATAR, F., 2016. Review article current investigations into magnetic nanoparticles for biomedical applications. *Journal of Biomedical Materials Research A*, **104**, 1285–1296.

LIANG, Y., BAI, P., ZHOU, J., WANG, T., LUO, B., and ZHENG S., 2016. An efficient precursor to synthesize various FeS_2 nanostructures via a simple hydrothermal synthesis method. *Crystal Engineering Communication*, **00**,1–3.

LIU, C., JI, Y., and TAN, T., 2013. One-pot hydrothermal synthesis of water-dispersible ZnS quantum dots modified with mercaptoacetic acid. *Journal of Alloys and Compounds*, **570**, 23–27.

LIU, F.K., KOA, F.H., HUANG, P.W., WUB, C.H., and CHU, T.H., 2005. Studying the size/shape separation and optical properties of silver nanoparticles by capillary electrophoresis. *Journal of Chromatography A*, **1062**, 139–145.

LUO, X., MORRIN, A., KILLARD, A.J., and SMYTH, M.R., 2006. Application of nanoparticles in electrochemical sensors and biosensors. *Electroanalysis*, **18**, 319–326.

MALIK, M.A, AFZAAL, M., O'BRIEN, P., BANGERT, U., and HAMILTON, B., 2004. Single molecular precursor for synthesis of GaAs nanoparticles. *Materials Science and Technology*, **20**, 959–963.

MALIK, M.A., REVAPRASADU, N. and O'BRIEN, P., 2001. Air-stable single-source precursors for the synthesis of chalcogenide semiconductor nanoparticles. *Chemistry of Materials*, **13**, 913–920.

MALIK, M.A, O'BRIEN, P. and REVAPRASADU, N., 1999. A novel route for the preparation of CuSe and $CuInSe_2$ nanoparticles. *Advanced Materials*, **11**, 1441–1444.

MALIK, M.A., O'BRIEN, P., and REVAPRASADU, N., 2002. Synthesis of TOPO-capped PtS and PdS nanoparticles from [Pt $(S_2CNMe(Hex))^2$] and [Pd $(S_2CNMe(Hex))^2$]. *Journal of material chemistry*, **12**, 92–97.

MANAHAN, S.E., 2009. *Fundamentals of sustainable chemical science*. Boca Raton: CRC Press.

MAO, B., DONG, D., EXSTROM, C.L., and HUANG, J., 2014. Surface thermal stability of iron pyrite nanocrystals: Role of capping ligands. *Thin Solid Films*, **562**, 361–366.

MATTOUSSI, H., AND CLAPP, A.R., 2008. Potential clinical applications of quantum dots. *International Journal of Nanomedicine*, **3**, 151–167.

NELWAMONDO, S.M.M., MOLOTO, M.J. and MOLOTO, N. 2012. M. Sc. (Chemistry) dissertation. [Unpublished]: University of Johannesburg. *Retrieved from: https://ujdigispace.uj.ac.za*. Johannesburg.

MASCIANGIOLI, T., and ZHANG, W., 2003. Environmental technologies at the nanoscale. *Environmental Science and Technology*, **37**,102A–108A.

MURTHY, S.K., 2007. Nanoparticles in modern medicine: state of the art and future challenges. *International journal of nanomedicine*, **2**, 129–41.

NANDA, J., SAPRA, S., and SARMA, D. D., 2000. Size-selected zinc sulfide nanocrystallites: Synthesis, structure, and optical studies. *Chemistry of Materials*, **12**, 1018–1024.

NATH, M. CHOUDHURY, A., KUNDU, A., and RAO, C.N.R., 2003. Synthesis and characterization of magnetic iron sulfide nanowires. *Advanced Materials*, **15**, 2098–2101.

NELWAMONDO, S.M.M., MOLOTO, M.J., KRAUSE, R.W.M., and MOLOTO, N., 2012. Synthesis and characterization of alanine-capped water soluble copper sulphide quantum dots. *Material Letters*, **75**, 161–164.

NYAMEN, L.D., NEJO, A.A., PULLABHOTLA,V.S.R., NDIFON, P.T., MALIK, M.A., AKHTAR, J., O'BRIEN, P and REVAPRASADU, N., 2014. The syntheses and structures of Zn(II) heterocyclic piperidine and tetrahydroquinoline dithiocarbamates and their use as single source precursors for ZnS nanoparticles. *Polyhedron*, **67**, 129–135.

OLUWAFEMI, O.S., and SONGCA, S.P., 2006. A facile one-pot synthesis of MSe (M = Cd or Zn) nanoparticles using biopolymer as a passivating agent. Dr. Johan Verbeek (Ed.), ISBN: 978-953-51-0226-7, InTech.

OLUWAFEMI, S.O., REVAPRASADU, N., and RAMIREZ, A.J., 2008. A novel one-pot route for the synthesis of water-soluble cadmium selenide nanoparticles. *Journal of*

Crystal Growth, **310**, 3230–3234.

PEER, D., KARP, J.M., HONG, S., FAROKHZAD, O.C., MARGALIT, R., and LANGER, R., 2007. Nanocarriers as an emerging platform for cancer therapy. *Nature Nanotechnology*, **2**, 751–760.

PEREIRO, R., COSTA-FERNÁDEZAND, J.M., SANZ-MEDEL, A., 2006. The use of luminescent quantum dots for optical sensing. *Trends in Analytical Chemistry*, **25**, 207–218.

PICKETT, N.L., and O'BRIEN, P., 2001. Syntheses of semiconductor nanoparticles using single-molecular precursors. *Chemical Records*, **1**, 467–479.

QUINTANA-RAMIREZ, P.V., ARENAS-ARROCENA, M.C., SANTOS-CRUZ, J., VEGA-GONZÁLEZ, M., MARTÍNEZ-ALVAREZ, O., CASTAÑO-MENESES, V.M., ACOSTA-TORRES, L.S., and FUENTE-HERNÁNDEZ, J., 2014. Growth evolution and phase transition from chalcocite to digenite in nanocrystalline copper sulfide: Morphological, optical and electrical properties. *Beilstein Journal of Nanotechnology*, **5**, 1542–1552.

RAHDAR, A., 2013. Effect of 2-mercaptoethanol as capping agent on ZnS nanoparticles : structural and optical characterization. *Journal of Nanostructure in Chemistry*, **3**,3–7

RAMASAMY, K., MALIK, M.A., REVAPRASADU, N., and O'BRIEN, P., 2013. Routes to nanostructured inorganic materials with potential for solar energy applications. *Chemistry of Materials*, **25**, 3551–3569.

RAO, C.N.R., KULKARNI, G.U., THOMAS, P.J., and EDWARDS, P.P., 2002. Size-dependent chemistry : Properties of nanocrystals. *Chemistry a European Journal*, **8**, 28–35.

REVAPRASADU, N., MALIK, M.A., O'BRIEN, P., WAKEFIELD, G., 1999. Deposition of zinc sulfide quantum dots from a single-source molecular precursor. *Journal of Materials Research*, **14**, 3237–3240.

ROGACH, A.L., KORNOWSKI, A., GAO, M., EYCHMULLER, A., and WELLER, H., 1999. Synthesis and characterization of a size series of extremely small thiol-stabilized CdSe nanocrystals. *The Journal of Physical Chemistry B*, **103**, 3065–3069.

ROY, P., MONDAL, K., and SRIVASTAVA, S.K., 2008. Synthesis of twinned CuS nanorods by a simple wet chemical method. *Crystal Growth and Design*, **8**, 1530–1534.

ROY, P., and SRIVASTAVA, S.K., 2007. Low-temperature synthesis of CuS nanorods by simple wet chemical method. *Materials Letters*, **61**, 1693–1697.

SAEED, S., RASHID, N., and AHMAD, K.S., 2013. Aerosol-assisted chemical vapor deposition of copper sulfide nanostructured thin film from newly synthesized single-source precursor. *Turkish Journal of Chemistry*, **37**, 796–804.

SALATA, O. V., 2004. Applications of nanoparticles in biology and medicine. *Journal of Nanobiotechnology*, **6**, 1–6.

SAMADI-MAYBODI, A., ABBASI, F., and AKHOONDI, R., 2014. Colloids and surfaces A : Physicochemical and engineering aspects aqueous synthesis and characterization of CdS quantum dots capped with some amino acids and investigations of their photocatalytic activities. *Colloids and Surfaces A: Physicochemical and Engineering Aspects*, **447**, 111–119.

SAMOILOVA, N., KURSKAYA, E., KRAYUKHINA, M., ASKADSKY, A., and YAMSKOV, I., 2009. Copolymers of maleic acid and their amphiphilic derivatives as stabilizers of silver nanoparticles. *Journal of Physical Chemistry*, **113**, 3395–3403.

SARANYA, M., and NIRMALA G., 2012. Hydrothermal synthesis of CuS nanostructures with different morphology. *Journal of Nano Research*, **18–19**, 43–51.

SATO, K., TACHIBANA, Y., HATTORI, S., CHIBA, T., and KAWABATA, S., 2008. Polyacrylic acid coating of highly luminescent CdS nanocrystals for biological labeling applications. *Journal of Colloid and Interface Science*, **324**, 257–260.

SCHER, E.C., MANNA, L., and ALIVISATOS, A.P., 2003. Shape control and applications of nanocrystals. *Philosophical Transactions of the Royal Society of London Series a-Mathematical Physical and Engineering Sciences*, **361**, 241–255.

SERVICE, R.F,.1884. Tiny particles flag scarce proteins. *Materials Science*, **301**, 1827.

SHARMA, D., KANCHI, S., and BISETTY, K., 2015. Biogenic synthesis of nanoparticles : A review. *Arabian Journal of Chemistry*, http://dx.doi.org/10.1016/j.arabjc.2015.11.002.

SHIOHARA, A., HOSHINO, A., HANAKI, K., SUZUKI, K., and YAMAMOTO, K., 2004. On the cyto-toxicity caused by quantum dots. *Microbiology and immunology*, **48**, 669–675.

SHUMBULA, P.M., MOLOTO, M. J., 2011, Synthesis and charactrization of water soluble sugar-capped metal sulphide semiconductor, PhD Thesis, School of Chemistry, Univbersity of the Witwatersrand.

SINGH, A., SHUKLA, R., SHANKER, R., and SINGH, S., 2015. Surface functionalization of quantum dots for biological applications. *Advances in Colloid and Interface Science*, **215**, 28–45.

SMITH, A.M., and NIE, S., 2009. Next-generation quantum dots. *Nature Biotechnology*, **27**, 732–733.

SOLTANI, N., SAION, E., ERFANI, M., REZAEE, K., BAHMANROKH, G., DRUMMEN, G.P.C., BAHRAMI, A., and HUSSEIN, M.Z., 2012. Influence of the polyvinyl pyrrolidone concentration on particle size and dispersion of ZnS nanoparticles synthesized by microwave irradiation. *International Journal of Molecular Sciences*, **13**, 12412–12427.

SONDI, I., SIIMAN, O., and MATIJEVIĆ, E., 2004. Synthesis of CdSe nanoparticles in the presence of aminodextran as stabilizing and capping agent. *Journal of Colloid and Interface Science*, **275**, 503–507.

SPANHEL, L., WELLER, H. and HENGLEIN, A., 1987. Photochemistry of semiconductor colloids. 22. Electron ejection from illuminated cadmium sulfide into attached titanium and zinc oxide particles. *Journal of the American Chemical Society*, **109**, 6632–6635.

SREEKUMARI N.P., RADHAKRISHNAN, T., REVAPRASADU, N., KOLAWOLE, G.A., and O'BRIEN, P., 2003. $Cd(NH_2CSNHNHCSNH_2)Cl_2$: A new single-source precursor for the preparation of CdS nanoparticles. *Polyhedron*, **22**, 3129–3135.

STOYANOVA, D.S., IVANOVA, I.A., and TODORKA, G., 2016. Nanobiotechnology against Salmonella spp. *Journal of Veterinary Madicine and Research*, **3**, 1057.

SUN, J.Q., SHEN, X.P., CHEN, K.M., LIU, Q., and LIU,W., 2008. Low-temperature synthesis of hexagonal ZnS nanoparticles by a facile microwave-assisted single-source method. Solid State Communications, **147**, 501–504.

SUN, X.L., CUI, W., HALLER, C., and CHAIKOF, E.L., 2004. Site-specific multivalent carbohydrate labeling of quantum dots and magnetic beads. *ChemBioChem*, **5**, 1593–1596.

TADJARODI, A., and KHALEDI, D., 2010. Preparation of CuS nanoparticles by

microwave irradiation, in: Proccedings of the 14th International Electronic Conference on Synthetic Orgnaic Chemistry, 1–5.

TALWATKAR, S.S., TAMGADGE, Y.S., SUNATKARI, A.L., GAMBHIRE, A.B., and MULEY, G.G., 2014. Amino acids (L-arginine and L-alanine) passivated CdS nanoparticles : Synthesis of spherical hierarchical structure and nonlinear optical properties. *Solid State Sciences*, **38**, 42–48.

TAMURA, J., FUKUDA, M., TANAKA, J., and KAWA, M., 2002. Synthesis of hydrophilic ultrafine nanoparticles coordinated with carbohydrate cluster. *Journal of Carbohydrate Chemistry*, **21**, 445–449.

TRINDADE, T., O'BRIEN, P. and PICKETT, N.L., 2001. Nanocrystalline semiconductors: Synthesis, properties, and perspectives. *Chemistry of Materials*, **13**, 3843–3858.

VANITHA, P. V. and O'BRIEN, P., 2008. Phase control in the synthesis of magnetic iron sulfide nanocrystals from a cubane-type Fe-S cluster. *Journal of the American Chemical Society*, **130**, 17256–17257.

VARSHNEY, M. and LI, Y., 2007. Interdigitated array microelectrode based impedance biosensor coupled with magnetic nanoparticle – antibody conjugates for detection of Escherichia coli O_{157} : H_7 in food samples. *Biosensors and Bioelectronics* , **22**, 2408–2414.

VAUGHAN, D.J., and CRAIG, J.R., 1978. Mineral chemistry of metal sulfides. *Earth-Science Reviews*, **15**, 494.

VIDYASAGAR, C.C., NAIK, Y.A., VENKATESHA, T. G., and VISWANATHA, R., 2012. Solid-state synthesis and effect of temperature on optical properties of CuO nanoparticles. *Nano-Micro Letters*, **4**, 73–77.

WAGNER, V., DULLAART, A., BOCK, A.K., and ZWECK, A., 2006. The emerging nanomedicine landscape. *Nature Biotechnology* , **24**, 1211–1217.

WALKER, B., 2000. Selected antimicrobial agents : mechanisms of action , side effects and drug interactions. *Periodontology*, **10**, 12–28.

WANG, E.C., and WANG, A.Z., 2015. Nanoparticles and their applications in cell and molecular boilogy. *Integrative Biology*, **6**, 9–26.

WANG, Y.S., THOMAS, P.J., and O'BRIEN, P., 2006. Nanocrystalline ZnO with ultraviolet luminescence. *Journal of Physical Chemistry B*, **110**, 4099–4104.

WATSON, H., 2015. Biological membranes. *Essays Biochem*, **59**, 43–69.

WEN, Z.-Q., LI, G., and REN, D., 2011. Detection of trace melamine in raw materials used for protein pharmaceutical manufacturing using surface-enhanced Raman spectroscopy (SERS) with gold nanoparticles. *Applied spectroscopy*, **65**, 514–521.

XIA, N., HUNT, T.P., MAYERS, B.T., ALSBERG, E., WHITESIDES, G.M.,WESTERVELT, R.M., and INGBER, D.E., 2006. Combined microfluidic-micromagnetic separation of living cells in continuous flow. *Biomedical Microdevices*, **8**, 299–308.

XIA, Y., YANG, H., and CAMPBELL, C.T., 2013. Nanoparticles for catalysis. *Accounts of Chemical Research*, **46**, 1671–1672.

YITAI, Q., YI, S., YI, X., QIANWANG, C., ZUYAO, C., and LI, Y., 1995. Hydrothermal preparation and characterization of nanocrystalline powder of sphalerite. *Materials Research Bulletin*, **30**, 601–605.

YU, W.W., CHANG, E., DREZEK, R., and COLVIN, V.L., 2006. Water-soluble quantum dots for biomedical applications. *Biochemical and Biophysical Research*

Communications, **348**, 781–786.

ZENG, X., and LIN, J., 2013. Beta-lactamase induction and cell wall metabolism in Gram-negative bacteria. , **4**, 1–9.

ZHANG, D., CARR, D.J., and ALOCILJA, E.C., 2009. Fluorescent bio-barcode DNA assay for the detection of *Salmonella enterica* serovar Enteritidis. *Biosensors and Bioelectronics*, **24**, 1377–1381.

ZHANG, L., PORNPATTANANANGKUL, D., HU, C.-M.J., and HUANG, C.-M. et al., 2010. Development of Nanoparticles for Antimicrobial Drug Delivery. *Current Medicinal Chemistry*,**17**, 585–594.

ZHANG, L., GU, F.X., CHAN, J.M., WANG, A.Z., LANGER, R.S., and FAROKHZAD, O.C., 2008. Nanoparticles in medicine: Therapeutic applications and developments. *Clinical Pharmacology and Therapeutics*, **83**, 761–769.

ZHANG, Y., LIU, Y., LI, C., CHEN, X., and WANG, Q., 2014. Controlled synthesis of Ag_2S quantum dots and experimental determination of the exciton Bohr radius. *The Journal of Physical Chemistry C*, **118**, 4918–4923.

ZHONG, X., HAN, M., DONG, Z., WHITE, T.J., and KNOLL, W., 2003. Composition-tunable $Zn_xCd_{1-x}Se$ nanocrystals with high luminescence and stability. *Journal of the American Chemical Society*, **125**, 8589–8594.

ZIELIŃSKA-JUREK, A., RESZCZYŃSKA, J., GRABOWSKA, E., and ZALESKA, A., 2011. Nanoparticles preparation using microemulsion systems, Microemulsions-An introduction to properties and applications, Dr. Reza Najjar (Ed.), ISBN: 978-953-51-0247-2, InTech.

Chapter 2

Research Methodology

---

2. Introduction

One of the most used method for the synthesis of nanoparticles is colloidal method. This method requires a reducing/capping agent for the formation of surface passivated nanoparticles. This method was used to improve the quality of nanoparticles and to control the water solubility of nanoparticles. A major goal of these methods is to produce high quality nanoparticles in a monodispersed form (i.e. with uniform/controllable size, shape and coefficient of variance) because the size and distribution of the particles are important factors that determine their physical and chemical properties. It is generally dependent on those properties. For example, the use of thiols, polymers, amino acids, surfactants and other ligands control particle size, shape and also prevent agglomeration. They can also introduce functionality to the surface of nanoparticles, an important feature for applications in nano-biology.

One of the challenges of preparing nanoparticles is to find a suitable method that would produce particles with a single phase and stoichiometry, high purity and monodispersity. FeS and CuS have a tendency of forming various phases, therefore careful control and choice of the reaction and its condition is essential. Herein, a simple but effective colloidal method adapted from a known method has been used (Tan *et al*. 2005). The colloidal synthesis involves the reaction of thioacetamide with a copper, zinc and iron salt with alanine, aspartic acid and lactose acting as a stabilizing agent. Alanine and aspartic acid are interesting molecules possessing two possible binding sites for the nanoparticles while lactose possess

one binding site to the surface of the nanoparticles. The reason for choosing such molecules is to ensure binding and stabilization of the semiconductor nanoparticles through one functional group while reserving the other for water solubility.

2.1 Materials

The following chemicals were purchased from Sigma-Aldrich (SA) and employed during this study without further purification: zinc chloride, copper chloride, iron chloride tetrahydrate, L-alanine, L-aspartic acid, lactose, sodium hydroxide, thioacetamide (TAA) and acetone.

2.1.1 Instrumentation

2.1.1.1 Fourier transform infrared spectroscopy

Fourier transform infrared (FTIR) samples were measured using Perkin Elmer Spectrum 400 FT-IR Spectrometer, universal ATR with diamond detector at wavelength from 650 cm^{-1} to 4000cm^{-1}.

2.1.1.2 Ultraviolet-visible Optical Spectroscopy

Ultraviolet-visible (UV-Vis) spectra of nanoparticle were obtained using a Perkin Elmer Lambda 25 UV/Vis, which collects spectra from 200-800nm UV and visible range using a slit of 1.0 and width of 0.1, using distilled water as a reference solvent.

2.1.1.3 Photoluminescence spectroscopy

The photoluminescence (PL) spectra were obtained using a Jasco-spectroflurometer FP-8600, which collects spectra from 200-800nm UV and visible range using a slit of 1.0 and width of 0.1.

2.1.1.4 X-Ray Powder Diffraction spectroscopy

The crystallographic characteristics of the nanoparticles were analysed by X-ray diffractometry (XRD) technique carried out on a Philips X'Pert materials research

diffractometer using a secondary graphite monochromated Cu Kα radiation (λ = 1.5406 Å) at 40 kV/50 mA. Samples were supported on a glass slides. Measurements were taken using a glancing angle of incidence detector at an angle of 2°, for 2θ values over 10°-80° in steps of 0.05°, with scan speed of 0.01° 2θ/s.

2.1.1.5 Transmission Electron Microscopy

Transmission electron microscope (TEM) images were obtained using a JEM-2100F at 200 kV. The TEM grids were prepared by depositing approximately 1 ml of the solution obtained after centrifugation and allowed to dry in air. The analysis were done in Mintek.

2.1.2 **Experimental procedure**

2.1.2.1 Synthesis of Cu_xS_y, ZnS and Fe_xS_y nanoparticles using L-alanine, L-aspartic acid and lactose.

The nanoparticles were synthesised using a modified method described by Tan *et al*. 2005. A typical synthesis experiment is described using the procedure for preparation of CuS nanoparticles capped with L-alanine as an example. L-Alanine (2.0018 g) was dissolved in (30 cm^3) of distilled water while stirring at room temperature. An aqueous copper(II) chloride solution (5 cm^3 of 0.744 M) was then added to the L-alanine solution and the pH of the mixture was adjusted to pH10 by adding aqueous sodium hydroxide (1 M). Aqueous thioacetamide (5 cm^3 of 1.33 M) was added to the mixture which was then heated at 35°C for 1 hour with vigorous stirring under nitrogen atmosphere. During this time a precipitation was formed. The mixture was allowed to cool to room temperature and the precipitate was isolated by centrifugation. The nanoparticles were washed several times with acetone and left overnight at room temperature to dry in a fume hood.

2.1.1.1 Cytotoxicity studies

Human cervical carcinoma cells (HeLa) are used to investigate *in vitro* cytotoxicity of nanoparticles using an MTS (3-(4,5-dimethylthiazol-2-yl)-5-(3-carboxymethoxyphenyl)-2-(4-sulfophenyl)-2H-tetrazolium) assay. HeLa cells were seeded (5 x 10^3 cells/well) in a 96-well plate in RPMI-1640 culture media supplemented with 10% calf serum and 1% penicillin/streptomycin. Cells were allowed to form a monolayer overnight in a 37°C incubator with 5% CO_2. Cells were then treated with fresh media containing nanoparticle suspension at different concentrations for 24 h at 37°C in the presence of 5% CO_2. After incubation, the media was removed from the wells and the wells were washed once with PBS. Twenty microliters of MTS reagent was added to each well and the plate was incubated for 4 h. Following incubation, the MTS reagent was replaced with 100 µl of an isopropanol-HCl solution and incubated for 1 h. After incubation, the plate was read in a UV plate reader at 570 nm. This test were performed at Mintek.

2.1.1.2 Antimicrobial activity studies

(a) Antibacterial activity

Minimum inhibitory concentrations (MIC) of the nanoparticles were determined using the microdilution bioassay as described by (Eloff 1998). In a typical experiment, overnight cultures of two Gram–positive (*Staphylococcus aureus* ATCC 25923 and *E. faecalis ATCC* 29212) and two Gram- negative (*Klebsiella pneumoniae* ATCC 13883 and *Pseudomonas aeruginosa* ATCC 15442) bacterial strains were diluted with sterile Mueller-Hinton (MH) broth to give final inoculums of approximately 10^6 CFU/mL. The nanoparticles were suspended in distilled water to give a concentration of 12.5 mg/mL. A 100 µL of each nanoparticle solution was serially diluted two-fold with sterile distilled water in a 96-well microtitre plate for each of the four bacterial strains. A two-fold dilution of neomycin (0.1

mg/mL) was used as a positive control against each bacterium. A 100 µL of each bacterial culture was added to each well and resazurin indicator was added in each well. Water and broth were included as negative controls. The plates were covered with lids and incubated at 37 °C for 24 hrs (Ncube *et al*. 2011). Wells with bacterial growth were indicated by the colour change observed from purple to pink or colourless. The lowest concentration of nanoparticles at which no colour change occurred was recorded as the MIC value. All the experiments were performed in triplicates.

(b) Antifungal activity

A microdilution method as described by Eloff (Eloff 1998) and modified for fungi by (Masoko *et al*. 2007) was used to determine the antifungal activity against *Candida albicans* (ATCC 14053) and *Cryptococcus neoformans* (ATCC 14116). In a typical experiment, an overnight fungal culture was prepared in yeast malt (YM) broth. A 400 µL of the overnight culture was added to 4 mL of sterile saline and absorbance was read at 530 nm. The absorbance was adjusted with sterile saline to match that of a 0.5 M McFarland standard solution. From this standardised fungal stock, a 1:1000 dilution with sterile YM broth was prepared to give a final inoculum of approximately 10^6 CFU/mL. The nanoparticles were suspended in distilled water to give a concentration of 12.5 mg/mL. A 100 µL of each nanoparticle solution was serially diluted two-fold with sterile distilled water in a 96-well microtitre plate. A similar two-fold dilution of Amphotericin B (2.5 mg/ml) was used as the positive control while water was used as negative and solvent controls respectively. A 100 µL of the diluted fungal culture was added to each well and resazurin solution was used as indicator. The plates were covered with lids and incubated at 37 °C for 24 hrs. The lowest concentration of nanoparticles at which no colour change occurred was recorded as the minimal fungicidal concentrations (MFC). All the experiments were performed in triplicates. The average values were calculated for the MFC of test material (Ncube *et al*. 2011).

2.2 References

ELOFF, J.N., 1998. A sensitive and quick microplate method to determine the minimal inhibitory concentration of plant extracts for acteria. *Planta Medica*, **64**, 711–713.

MASOKO, P., PICARD, J., and ELOFF, J.N., 2007. The antifungal activity of twenty-four Southern African Combretum species (Combretaceae). *South African Journal of Botany*, **73**, 173–183.

NCUBE, B., FINNIE, J.F. and STADEN, J. VAN., 2011. Seasonal variation in antimicrobial and phytochemical properties of frequently used medicinal bulbous plants from South Africa. *South African Journal of Botany*, **77**, 387–396.

TAN, C., ZHU, Y., LU, R., XUE, P., BAO, C., LIU, X., FEI, Z., and ZHAO, Y., 2005. Synthesis of copper sulfide nanotube in the hydrogel system. *Materials Chemistry and Physics*, **91**, 44–47.

Chapter 3

Bio-functionalized Cu_xS_y, ZnS and Fe_xS_y nanoparticles

3.1 Background

Nanostructured transition metal chalcogenides are very interesting materials at present due to their unique chemical and physical properties compared to the bilk materials. The size and surface-dependent properties of nanoparticles have stimulated research on their surface modification with an aim to broaden their potential applications. Intensive research on nanoparticles over the past decade has focused on the study of their optical and electrical properties for possible applications in biological labels, optoelectronic devices, photovoltaic cells and lasers (Rogach & Weller 2000; Barnham *et al*. 2013).

For the past decade, functionalization of semiconductor nanoparticles with biomolecules through biosynthesis of semiconductors (Wang *et al*. 2002; Ahmad *et al*. 2002), and metal nanoparticles (Sibiya *et al*. 2016), with bio-molecules such as starch, proteins and nucleic acids (Sutherland 2002), has added a new element to research at the nanoscale level. The bio-functionality of the nanoparticles facilitates selective interaction with target biochemical species, thereby extending the area of applications to the biological or chemical system (Oluwafemi *et al*. 2008), for example, the preparation of nonradioactive biological labels (Bruchez *et al*. 1998) and chemical optosensors (Murphy 2002).

The most recent advances in the applications of nanoparticles are in the field of biology. With bright, photostable fluorescence, these semiconductor nanoparticles or quantum dots (QDs) show promise as alternatives to organic dyes for fluorescent biology labeling (Bruchez *et al*. 1998). However, the difficulty in producing stable QDs-biomolecules

complexes has slowed down the development of QDs in biological labeling (Pereiro & Sanz-medel 2006). In addition to biological applications, it is highly essential for high-quality water-soluble semiconductor nanoparticles. Since the pioneering work of Chan and Nie (Chan & Nie 1998), and Bruchez *et al*. (Bruchez *et al*. 1998), semiconductor nanoparticles were made biocompatible and water soluble *via* surface coating. Various methods have been developed in which water-soluble semiconductor nanoparticles can be synthesized directly in one-pot (Lai *et al*. 2010).

In this chapter, the syntheses of bio-functionalized copper sulphide (CuS), zinc sulphide (ZnS) and iron sulphide (FeS) nanoparticles using L-alanine, L-aspartic and lactose as a capping agent is reported. L-Alanine for example, is the smallest, naturally occurring chiral amino acid with a non-reactive hydrophobic methyl group as a side chain. Depending on the reaction medium, L-alanine molecules can be stabilized in different forms, namely, cationic, anionic and zwitterionic (Nelwamondo *et al*. 2012). The presence of these in solution depend mainly on pH. Above pH 9, more than 90% of L-alanine molecules in aqueous solution are found in the form of anionic, whereas below pH 1.5, more than 90% are in the cationic form. In the pH ranges from 4.5 to 7.5, approximately 99% of L-alanine molecules become fully zwitterionic (Nelwamondo *et al*. 2012). The choice of two amino acids and one disaccharide was to evaluate the effect of chain length, reactivity of two functional groups for amino acids (-COOH and NH), and stability. In this study, pH 10 was chosen with the aim of utilizing the anionic hydroxyl moiety that can bind to the surface of the nanoparticles.

3.2 Results and discussion

3.2.1 L-alanine as capping agent for CuS, ZnS and FeS nanoparticles

One of the challenges of preparing nanoparticles is to find a suitable method that would produce particles with a single phase and stoichiometry, high purity and monodispersity. CuS and FeS have tendencies of forming various phases. Therefore, careful control, choice of the reaction, and conditions are vital. Herein, a simple but effective colloidal method adopted from (Tan *et al.* 2005) has been used. The colloidal synthesis involves the reaction of thioacetamide with either copper, zinc or iron chloride, and also L-alanine acting as a capping agent. L-Alanine is an interesting molecule possessing two possible binding sites for the nanoparticles as shown in scheme 3.1(I).

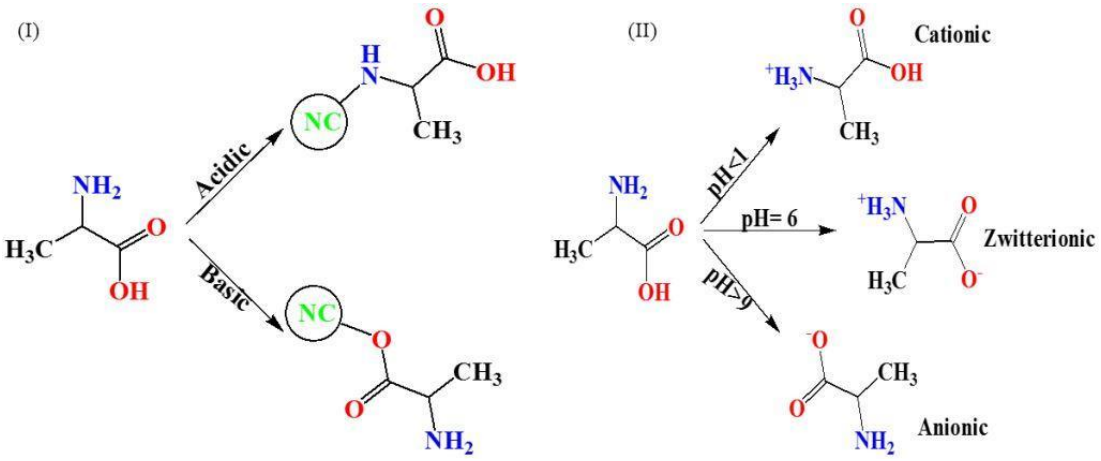

Scheme 3.1. Representation of the (I) binding motifs of L-alanine on the surface of metal sulfide nanoparticles and (II) effect of pH on L-alanine in an aqueous medium.

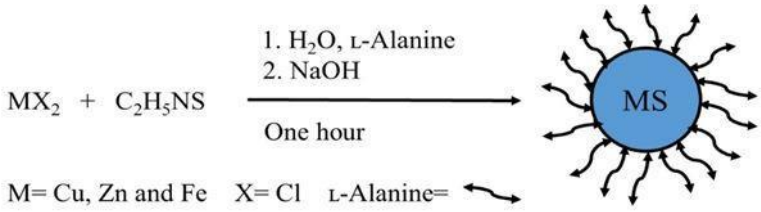

Scheme 3.2. Representation of the formation of L-alanine-capped CuS, ZnS and FeS nanoparticles.

3.2.1.1 Interaction between L-alanine and the nanoparticles

FTIR spectroscopy was used to identify the functional groups of the active components. Fig. 3.1 shows the FTIR spectra of L-alanine and the prepared L-alanine-capped-CuS, ZnS and FeS nanoparticles. L-Alanine (Fig. 3.1(a)) has characteristic overlapping bands at 2500 and 3108 cm^{-1} which are assigned to O-H and $N-H^{3+}$ stretching, respectively. In addition, there are peaks around 1600 cm^{-1} and 1149 cm^{-1} assigned to the C=O bond and C-O band. Fig. 3.1 (b) shows the spectrum of L-alanine capped CuS nanoparticles with a band around 3250 cm^{-1} associated with the $N-H^{3+}$ stretching frequency. The existence of the above band suggests the bonding of L-alanine to the surface of CuS nanoparticles through the negatively charged hydroxyl moiety. The $N-H^{3+}$ band of L-alanine capped CuS nanoparticles was more noticeable compared to the pristine alanine because the bonds are constrained at the surface of the nanoparticles.

The other differences observed were on the C=O and C-O (1600 and 1280 cm^{-1}) bands which shifted to higher frequencies compared to the pristine alanine (1576 cm^{-1} and 1149 cm^{-1}). These differences arise from the electron density being delocalised within the O-C-O moiety which confirms that the bonding of L-alanine to the surface of the nanoparticles occurred through basic route in Scheme 3.1. In addition, the difference between the free L-alanine and L-alanine-capped CuS nanoparticles indicates that the L-alanine molecules have been chemisorbed through the hydroxyl moieties onto the surface of nanoparticles. The IR spectra of the L-alanine capped ZnS and FeS nanoparticles (Fig. 3.1 (c and d) has a broad band around 3253 cm^{-1} associated with N-H stretching mode of L-alanine. This broad $N-H^{3+}$ band was also reported by other researchers (Nelwamondo *et al*. 2012; Oluwafemi *et al*. 2008; Lee *et al*. 2009). In addition, the C=O stretching mode around 1600 cm^{-1} was broader as compared to that of free L-alanine because the bonds are strained due to bonding to the

surface of nanocrystals. These observations confirm that the nanoparticles were capped with L-alanine.

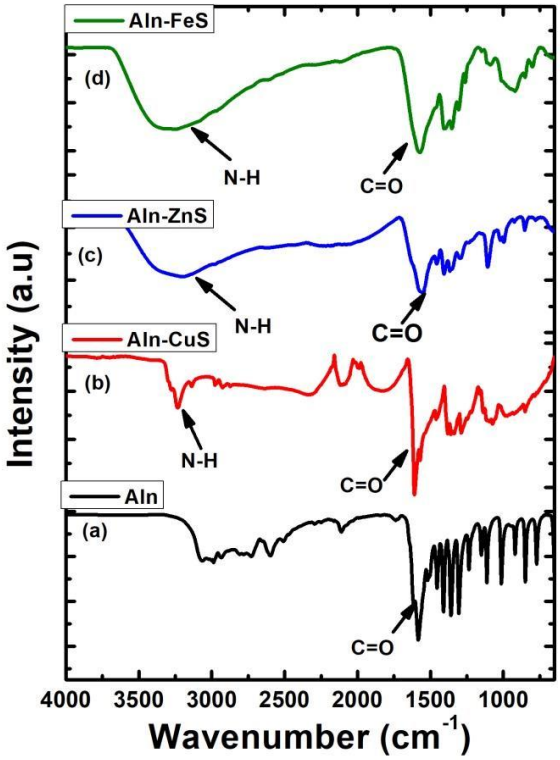

Figure 3.1. Infrared spectra of (a) free L-alanine, L-alanine-capped (b) CuS, (c) ZnS and (d) FeS nanoparticles.

3.2.1.2 Ultraviolet-visible and Photoluminescence spectroscopic characterization of nanoparticles

The study of optical absorption is important to understand the behavior of semiconductor nanoparticles. A fundamental property of semiconductors is the band gap, the energy separation between the filled valence band and the empty conduction band. Optical excitation of electrons across the band gap is strongly allowed, producing a sharp increase in absorption at the wavelength corresponding to the bandgap energy (Eg). This feature in the optical spectrum is known as the optical absorption edge.

Fig. 3.2 (I, II, III) shows the UV-Vis absorption spectra of CuS, ZnS and FeS nanoparticles capped with L-alanine, synthesized at different temperatures. All absorption spectra are blue-shifted to their corresponding bulk, which are 1022 (CuS), 345 (ZnS) and 510 to 1378 nm (FeS). This is as a result of the quantization of the energy levels in the valence and conduction bands of the nanoparticles causing an increase of the band-gap energy. CuS nanoparticles (Fig. 3.2 (I)) absorb in the region of 300–650 nm. In addition to that, the spectra show another broad band in the near-IR region, which is the characteristic band for covellite CuS (Roy & Srivastava 2007). Fig 3.2 (II) is the UV-Vis absorption spectra of ZnS nanoparticles. For the lowest synthetic temperature (35 °C), a well-resolved excitonic peak was observed at 257 nm, which corresponds to the $1S_e$-$1S_h$ excitonic transition in the ZnS nanoparticles (Wang *et al*. 2006). In addition, there is a sharp absorption edge at 308 nm, which is at a shorter wavelength than 345 nm of the bulk ZnS indicating small sizes.

In the absorption spectra of FeS nanoparticles (Fig 3.2 (III)), sharp excitonic peaks appearing at approximately 258 nm were observed in all temperatures. In addition to those excitonic peaks, broad shoulders appearing between 300 and 450 nm were also observed. The excitonic peak suggests that the particles have a narrow size distribution, while a shoulder like absorption had a higher degree of tailing and thus made it difficult to accurately locate the band edges for all three samples. However for all samples as the temperature was increased from 35 to 65, and then 95 °C, the band edges were observed to be shifting to higher wavelength, signifying an increase in particles size. Table 3.1 presents the band edges of the as-synthesized CuS, ZnS and FeS nanoparticles capped with L-alanine.

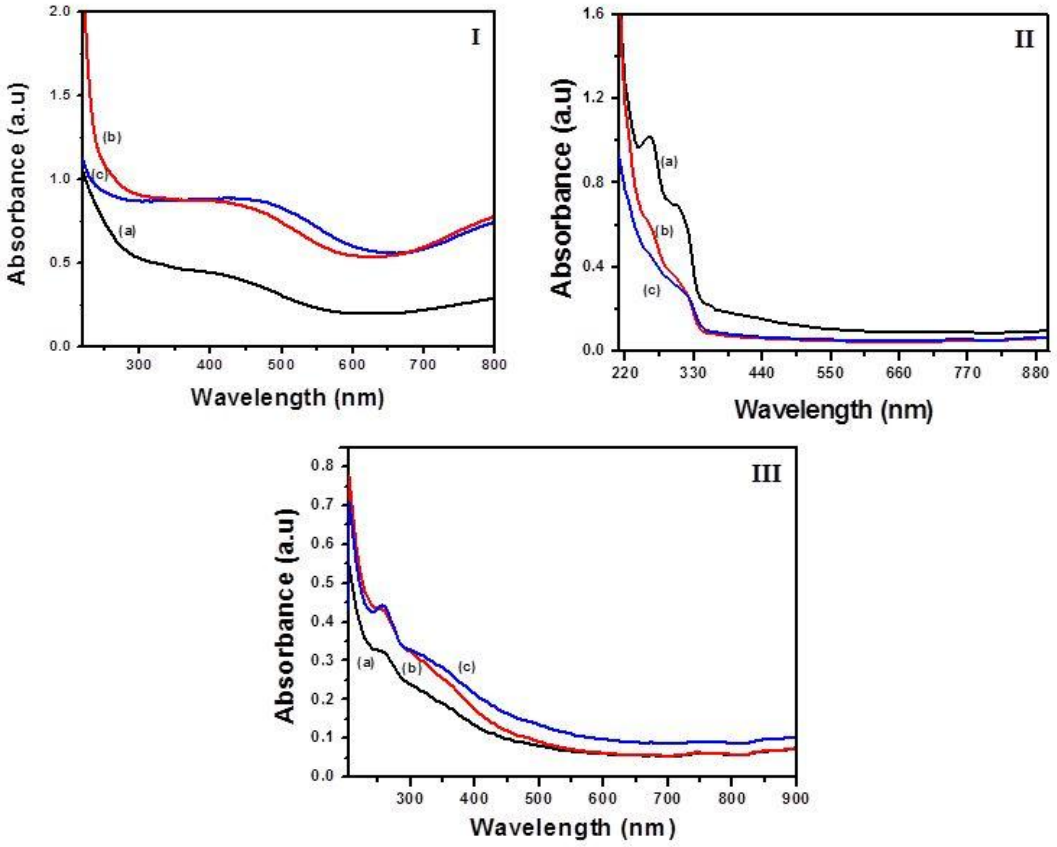

Figure 3.2. UV–Vis absorption spectra of L-alanine-capped (I) CuS, (II) ZnS and (III) FeS nanoparticles synthesized at (a) 35 °C, (b) 65 °C and (c) 95 °C.

Table 3.1. Band edges of L-alanine-capped CuS, ZnS and FeS nanoparticles synthesised at different temperatures.

Temperature (°C)	Band edges (nm)		
	CuS	ZnS	FeS
35	564	339	428
65	590	340	445
95	636	343	497

The emission spectra of nanoparticles, on the other hand, depend on surface state, size and surface passivation. Fig. 3.3 (I, II, III) shows the emission spectra of synthesized CuS, ZnS and FeS nanoparticles samples dispersed in distilled water. The samples for CuS were excited at a wavelength of 275 nm, while ZnS and FeS samples were excited at a wavelength of 300 nm. The emission maxima for all samples are shown in Table 3.2. All spectra became broader as the temperature increased from 35 to 95 ^{o}C, signifying formation of bigger particles size and polydispersity. A significant shift to higher wavelength was observed as the temperature was increase, with the exception of Fig 3.3 (III, b and c). An increase to higher wavelength agrees well with the results obtained in the absorption spectra where the band edge increased with increase in temperature.

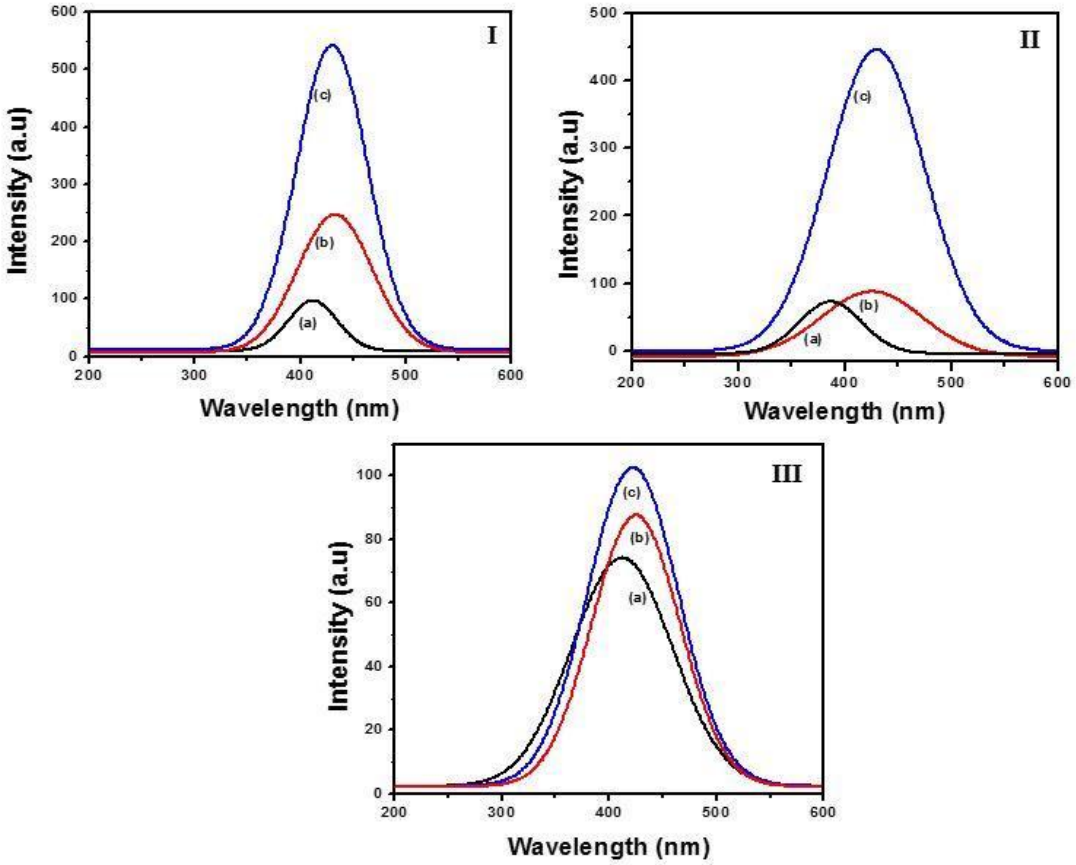

Figure 3.3. Photoluminescence spectra of L-alanine-capped (I) CuS, (II) ZnS and (III) FeS nanoparticles synthesized at (a) 35 °C, (b) 65 °C and (c) 95 °C.

Table 3.2. Emission maxima of synthesized CuS, ZnS and FeS nanoparticles at different temperatures.

Temperature (°C)	Emission maxima (nm)		
	CuS	ZnS	FeS
35	412	384	413
65	384	425	425
95	413	430	423

3.2.1.3 Structural characterization

The crystalline nature of nanoparticles was confirmed by XRD. Fig. 3.4 (I, II, III) shows the XRD patterns of the synthesised L-alanine-capped CuS, ZnS and FeS nanoparticles prepared at different temperatures. The resultant products for CuS nanoparticles (Fig.3.4 (I)) are of pure since there are no peaks due to impurities. The diffraction peaks at 2θ values of 32.23°, 34.10°, 37.05°, 45.38°, 50.45°, 56.24°, 62.01°, 67.43° and 70.09° corresponding to miller indices (101), (102), (103), (105), (106), (110), (108), (202) and (116), respectively, were closely indexed with the standard peaks of hexagonal phase of CuS covellite (JCPDS no: 06-0464) (Saranya *et al*. 2014). The XRD patterns for ZnS nanoparticles (Fig. 3.4 (II)) exhibited three diffraction peaks at 2θ values of 33.3°, 55.8°, and 66.7°, corresponding to miller indices (111), (220), and (311) planes of the cubic zinc sulfide blend phase. No extra peaks were found, indicating a pure and single phased nature of the nanoparticles. The diffraction pattern was in good agreement with the JCPDS card of ZnS (JCPDS no: 01-072-4841) (Othman *et al*. 2014). FeS nanoparticles were closely indexed to the cubic greigite (Fe_3S_4) (ICDD No: 00-016-0713) (Akhtar & O'Brien 2013).

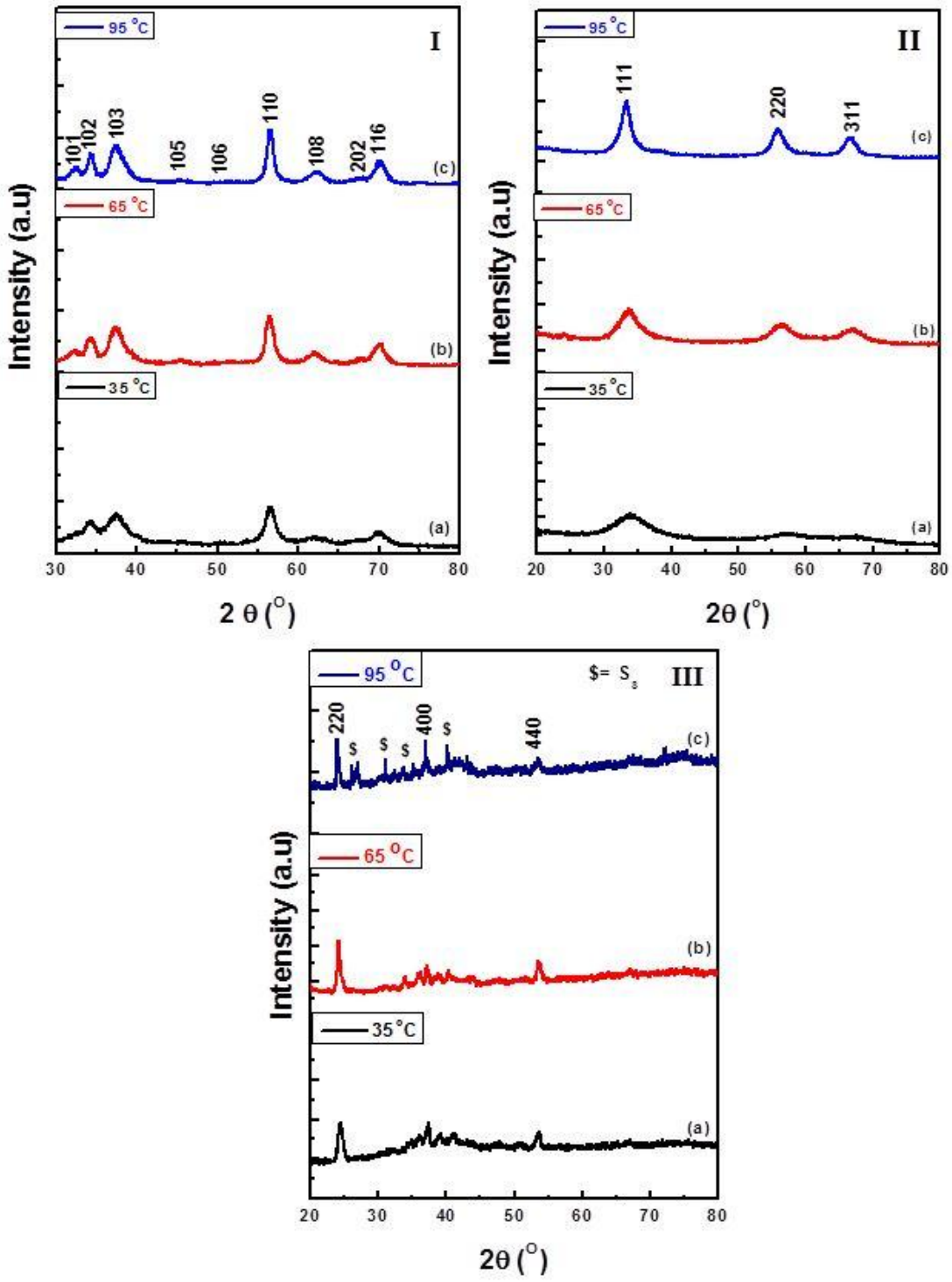

Figure 3.4. XRD patterns of L-alanine-capped (I) CuS, (II) ZnS and (III) FeS nanoparticles synthesized at (a) 35 °C, (b) 65 °C and (c) 95 °C.

However, there were peaks of impurities corresponding to rosickyite S_8 (ICDD No: 00-053-1109). This shows that the reactants were not completely converted to the products. The broadness of peaks indicates the formation of small sizes. On increasing the reaction temperature, the intensity of peaks increased indicating the formation of a highly crystalline/ bigger particles at a higher temperature. In addition, the narrowness of the peaks with an increase in reaction temperature was attributed to Oswald ripening.

Fig 3.5(I) shows the TEM images of L-alanine-capped CuS nanoparticles synthesized at 35, 65 and 95 °C. The particles obtained for all three set of temperatures had mixed morphology, i.e., rod and irregular-shaped nanoparticles, with rod-shaped particles dominating. The synthesized CuS nanoparticles at 35 °C depicted rod-shaped particles with an average diameter of 3 nm and an average length of 17 nm. As the temperature was increased to 65 °C, both diameter and length were affected, depicting an average diameter of 6 nm, while average length obtained was 23 nm. A further temperature increase to 95 °C depicted rod-shaped particles with an average diameter and length of 8 and 33 nm, respectively.

For ZnS nanoparticles (Fig. 3.4(II)) the images revealed some agglomeration of uniformly distributed close-to-spherical nanoparticles, with an average diameter of 6.09, 6.53 and 9.45 nm for sample synthesized at 35, 65 and 95 °C, respectively. With regards to FeS nanoparticles (Fig. 3.4(III)), the images revealed some mixed morphology of rod-shaped dominated by close-to-spherical iron sulfide nanoparticles with an average particles size of 2.36, 2.63 and 3.03 nm for samples synthesized at 35, 65 and 95 ºC, respectively.

For all samples, no change in morphology was affected as the temperature was increased. The increase in particle size with increase in reaction temperature was attributed to Oswald ripening. The TEM results support the data or results obtained above in the absorption and emission spectra, together with their XRD spectroscopy.

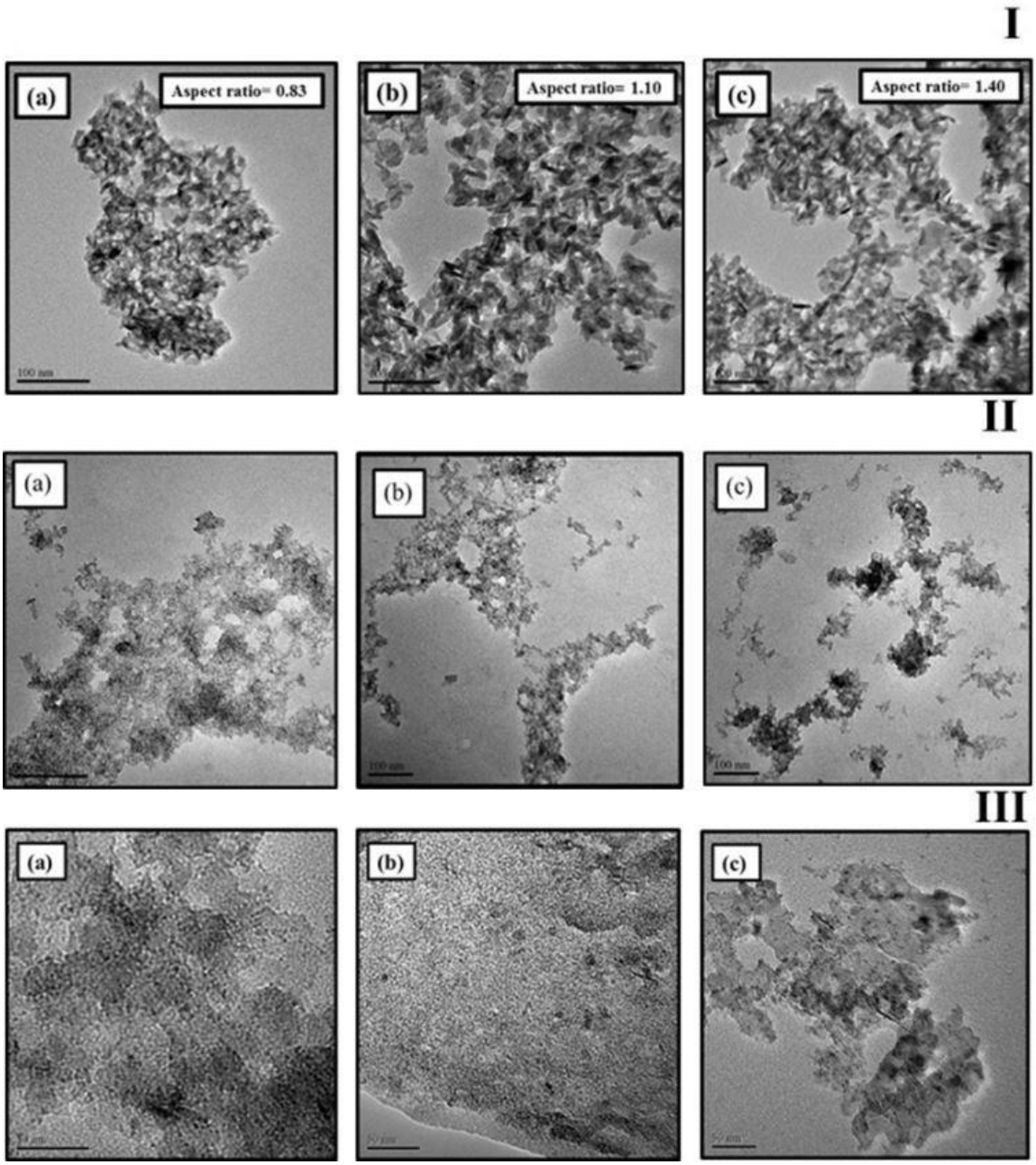

Figure 3.5. TEM images of L-alanine-capped (I) CuS, (II) ZnS and (III) FeS nanoparticles synthesized at (a) 35 °C, (b) 65 °C and (c) 95 °C.

To further investigate the surface properties of the nanoparticles, a solubility test was performed in triplicates for each metal sulfide nanoparticles synthesized at 35, 65 and 95 °C. An equal amount of 0.0074 g nanoparticles synthesized at the various temperatures was dissolved in an equal amount of distilled water (5 cm^3) and sonicated at room temperature

for 60 min and centrifuged. The average concentration was then measured to establish the solubility of the particles. The concentration was measured by subtracting the mass of un-dissolved particles from the initial mass (0.0074 g) (Nelwamondo *et al*. 2012). The solubility increased with an increase in synthetic temperature for all CuS, ZnS and FeS nanoparticles. This could be due to that as the temperature was increased the particles size also increase as seen in XRD peaks becoming sharper and visible with an increase in temperature. The solubility of all the particles confirms the coating of the surface of the nanoparticles with L-alanine. At 95 °C, most of the particles were soluble in water; this indicates that this synthetic temperature is the best condition for L-alanine-capped CuS, ZnS and FeS nanoparticles.

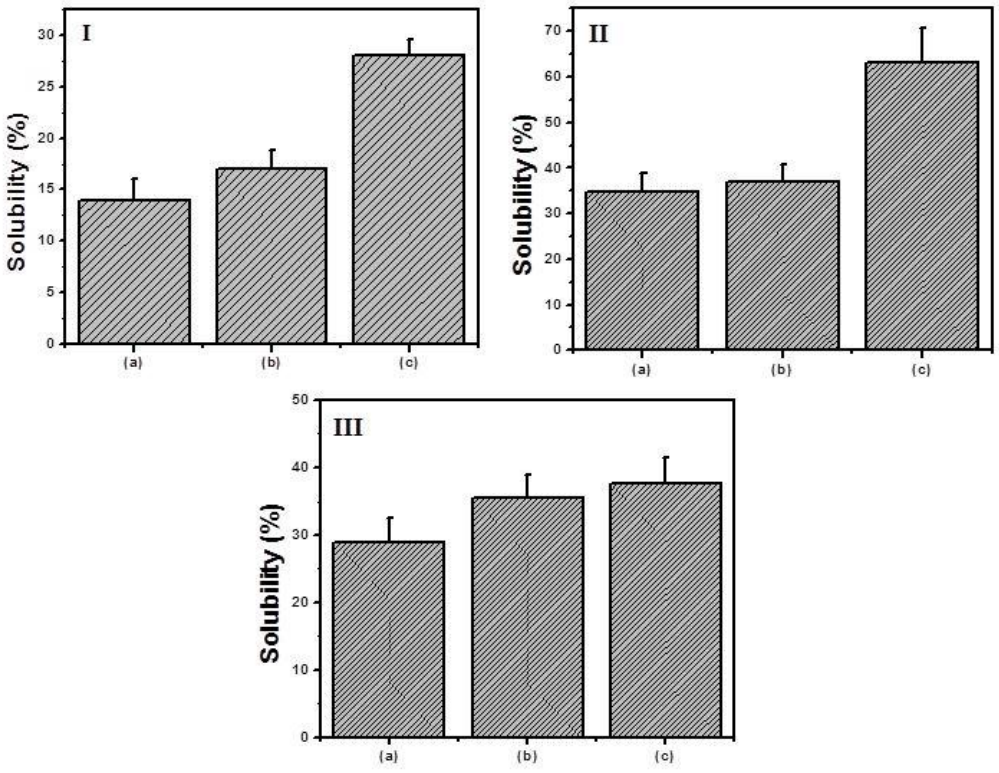

Figure 3.6. Water solubility graph of L-alanine-capped (I) CuS, (II) ZnS and (III) FeS nanoparticles synthesized at (a) 35 °C, (b) 65 °C and (c) 95 °C.

3.2.2 *L-aspartic acid as capping agent for CuS, ZnS and FeS nanoparticles*

L-Aspartic acid-capped metal sulfide nanoparticles were synthesised using colloidal aqueous synthetic route. The reaction temperature of the L-aspartic acid-capped metal sulfide nanoparticles was varied to see the effect on the morphology and size of the nanoparticles formed. L-Aspartic acid contains ionizable carboxylic and amine functional groups and this amino acid moiety is responsible for the water solubility nature of the nanoparticles formed.

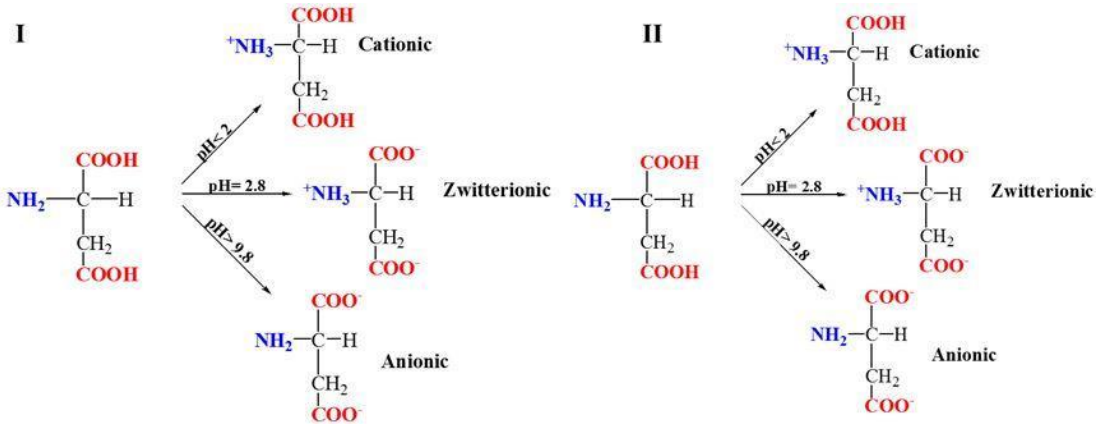

Scheme 3.3. Representation of the (I) binding motifs of L-aspartic acid on the surface of metal sulfide nanoparticles and (II) effect of pH on L-aspartic acid in an aqueous medium.

3.2.2.1 Interaction between L-aspartic acid and nanoparticles

The L-aspartic acid molecules attached to the surface of the nanoparticles were characterized by FTIR spectroscopy. Fig 3.7 presents the FTIR spectra of L-aspartic acid-capped CuS, ZnS and FeS nanoparticles. Table 3.3 presents the obtained peak data and their assignments. These specific vibrational modes were assigned by comparison with previously reported assignments of the FTIR spectra of free L-aspartic acid reported by other researchers (Alam & Ahmad 2012; Rajkumar *et al*. 1998). In the spectra, free L-aspartic acid (Fig. 3.7 (a)) has characteristic overlapping bands between 2500 and 3100 cm^{-1} which are assigned to O-H

and N-H stretching, respectively. In addition, the peak around 1500 cm^{-1} was assigned to the C=O stretching. Fig. 3.7 (b) shows the spectra of L-aspartic acid capped CuS nanoparticles with a band appearing at 3060 cm^{-1}, which is associated with the N-H stretching frequency. In contrary, the FTIR spectra of L-aspartic acid-capped ZnS and FeS (Fig. 3.7 (c and d)) nanoparticles exhibited a broad peak centered at 3250 cm^{-1}, which was assigned to the O-H stretching mode of water. The most characteristic peak of the L-aspartic acid-capped nanoparticles was the C=O stretching peaks appearing at 1580 cm^{-1}. The carbonyl peak for the pristine L-aspartic acid is less intense and narrower compared to the L-aspartic acid capped nanoparticles.

The broadness of L-aspartic acid capped nanoparticles might be due to the electron density of L-aspartic acid molecules being distributed to a much heavier metal ions on the surface of the nanoparticles (Heo & Hwang 2016). The overall peaks obtained from L-aspartic acid-capped ZnS nanoparticles were slightly shifted towards lower wavenumbers compared to those of the pristine L-aspartic acid molecule, since some of the vibrational modes were restricted by attaching to a much heavier transition metal ions (Cu^{2+}, Zn^{2+}, and Fe^{2+}) on the surface of the nanocrystal lattice (Heo & Hwang 2016). Therefore, according to these assignments, carboxylic moieties of the pristine L-aspartic acid molecule were attached to the nanoparticles surface, while the amine moiety remained uncoordinated to impart a hydrophilic nature to the nanoparticles.

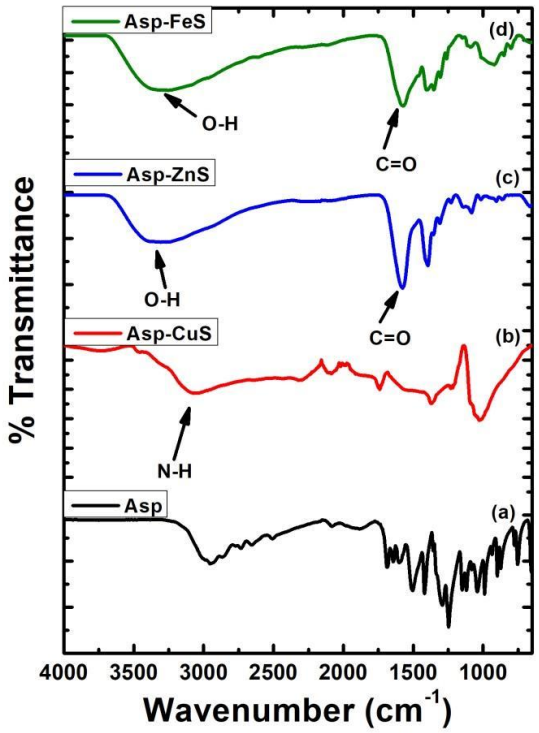

Figure 3.7. Infrared spectra of (a) pristine L-aspartic acid, L-aspartic acid-capped (b) CuS, (c) ZnS and (d) FeS nanoparticles.

Table 3.3. FTIR data and assignments of L-aspartic acid-capped CuS, ZnS and FeS nanoparticles.

L-Aspartic acid-capped nanoparticles (cm^{-1})	Pristine L-aspartic acid (cm^{-1})	Assignments
526	524	□(C-C-O)
904	894	ρ(C-C)
1082	1046	ν(C-N)
1309	1312	□(O-H)
1372, 1402	1420	ν (OCO) + □ (C-O)
1586, 1600	Did no appear	ν (C=O-M)
3350, 3290	2952	ν (O-H, H_2O)

(ν -stretching; □-in-plane deformation; ρ-rocking).

3.2.1.1 Ultraviolet-visible and Photoluminescence spectroscopic characterization of nanoparticles

The absorption spectra of L-aspartic acid-capped CuS, ZnS, and FeS nanoparticles are shown in Fig. 3.8 (I, II, III). All absorption spectra are blue-shifted to their corresponding bulk, signifying small sizes of the nanoparticles. The absorption spectra of the prepared CuS nanoparticles (Fig. 3.8 (I)) depict a broad band in the region between 366–595 nm. The optical excitonic peaks for ZnS nanoparticles (Fig 3.8 (II)) are located at approximately 330 nm suggesting narrow size distribution and good passivation of nanoparticles by L-aspartic acid.

In the case of FeS nanoparticles (Fig 3.8 (III)), a shoulder with a high degree of tailing appearing at approximately 360 nm, was observed for all samples synthesized at different temperatures. The appearance of this shoulder might result due to poor passivation of nanoparticles which leads to particles aggregation. Nevertheless, the band-edges were extrapolated by a tangent through the midpoint of the turning point of the curves and the optical data is tabulated in Table 3.4. As the temperature was increased from 35 to 65, and then 95 °C, the band edges were observed to be shifting to higher wavelength for all samples, implying an increase in particles size.

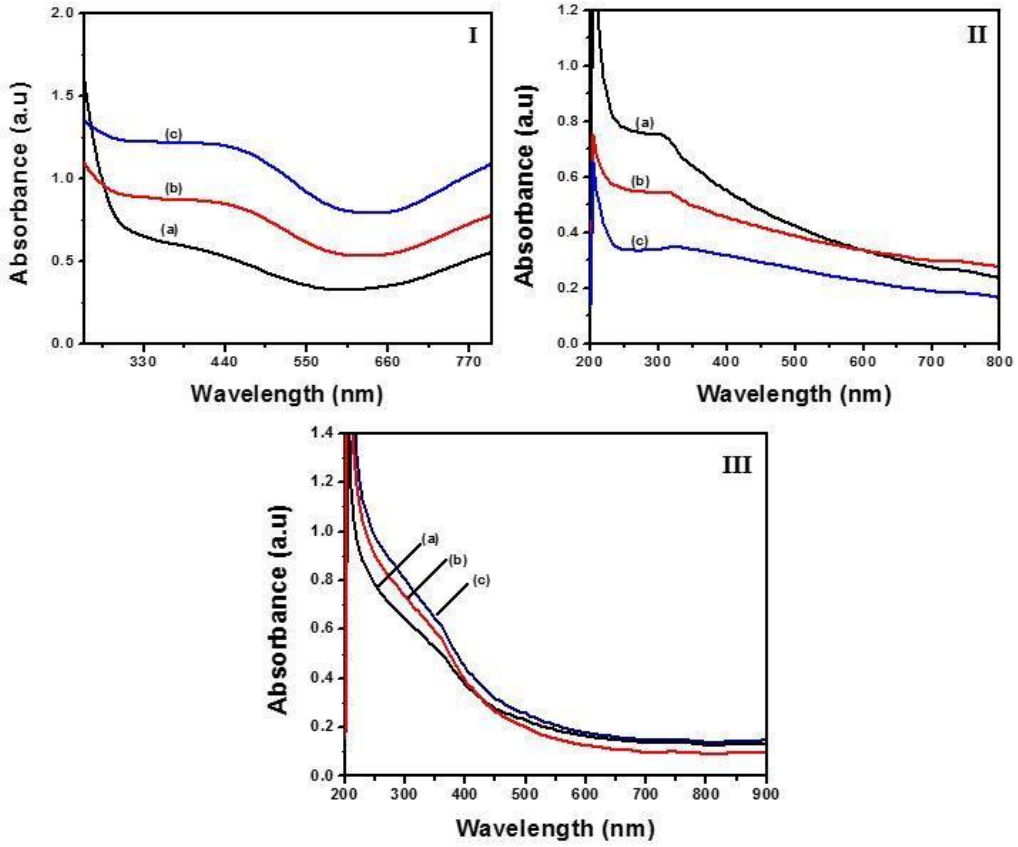

Figure 3.8. UV–Vis absorption spectra of L-aspartic acid-capped (I) CuS, (II) ZnS and (III) FeS nanoparticles synthesized at (a) 35 °C, (b) 65 °C and (c) 95 °C.

Table 3.4. Band edges of L-aspartic acid-capped CuS, ZnS and FeS nanoparticles synthesised at different temperatures.

Temperature (°C)	Band edges (nm)		
	CuS	ZnS	FeS
35	541	308	352
65	564	319	358
95	587	328	230

Fig. 3.9 shows the emission spectra of L-aspartic acid-capped CuS, ZnS and FeS nanoparticles prepared at different temperatures. The spectra for all samples depict a well-defined emission bands with the emission maximum peaks located at different wavelengths, as can be seen in Table 3.5. The noticeable differences in the spectra are the red-shift for CuS and FeS nanoparticles synthesized at 95 °C as compared to lower temperatures, which could be attributed to the different reaction temperature used in their preparation. The emission peaks of ZnS and FeS nanoparticles were due to the trap-state emission, rather than the band-edge emission because of the large stoke shifts. The trap-state emission is associated with the electron being trapped between the conduction band and the valence band due to surface defects.

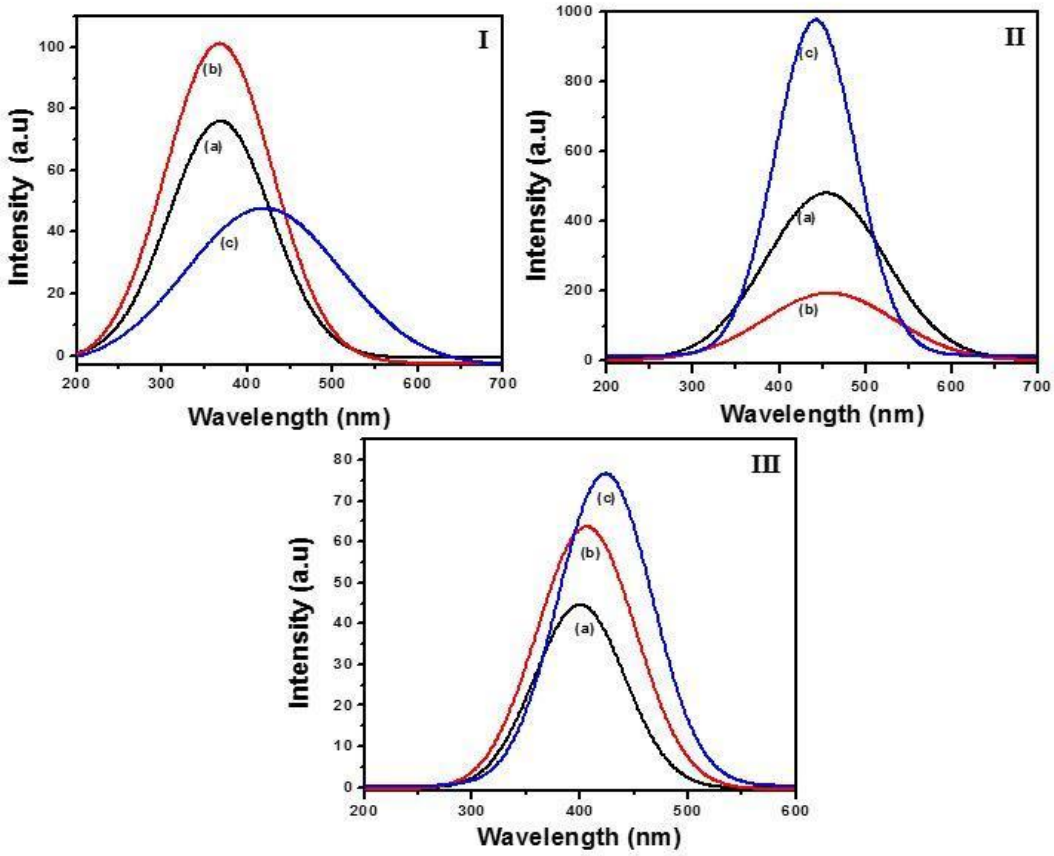

Figure 3.9. Photoluminescence spectra of L-aspartic acid-capped (I) CuS, (II) ZnS and (III) FeS nanoparticles synthesized at (a) 35 °C, (b) 65 °C and (c) 95 °C.

Table 3.5. Emission maxima of synthesized CuS, ZnS and FeS nanoparticles at different temperatures.

Temperature (°C)	Emission maxima (nm)		
	CuS	ZnS	FeS
35	366	368	400
65	452	458	406
95	400	442	424

3.2.1.2 Structural properties

The XRD patterns of L-aspartic acid-capped CuS, ZnS and FeS nanoparticles synthesized at 35, 65 and 95 °C are shown in Fig. 3.10. All the diffraction peaks for CuS and ZnS samples confirmed the crystalline nature of the synthesized materials which are made with nano-size level particles. The peaks for CuS samples (Fig. 3.10 (I)) were indexed to hexagonal phase of CuS covellite (JCPDS no: 06-0464), while the peaks for ZnS samples (Fig. 3.10(II)) were indexed to a cubic zinc sulfide blend (JCPDS no: 01-072-4841). In contrary, the absences of the significant peaks for FeS nanoparticles (Fig. 3.10 (III)) demonstrate that the materials synthesized are amorphous. This could be due to the method used for preparation which did no favor a crystalline material for FeS. An increase in reaction temperature for CuS and ZnS samples resulted in slight increase in crystallinity, with the diffraction peaks becoming narrower, indicating bigger particle sizes. The narrowness of the peaks with an increase in reaction temperature was attributed to Oswald ripening.

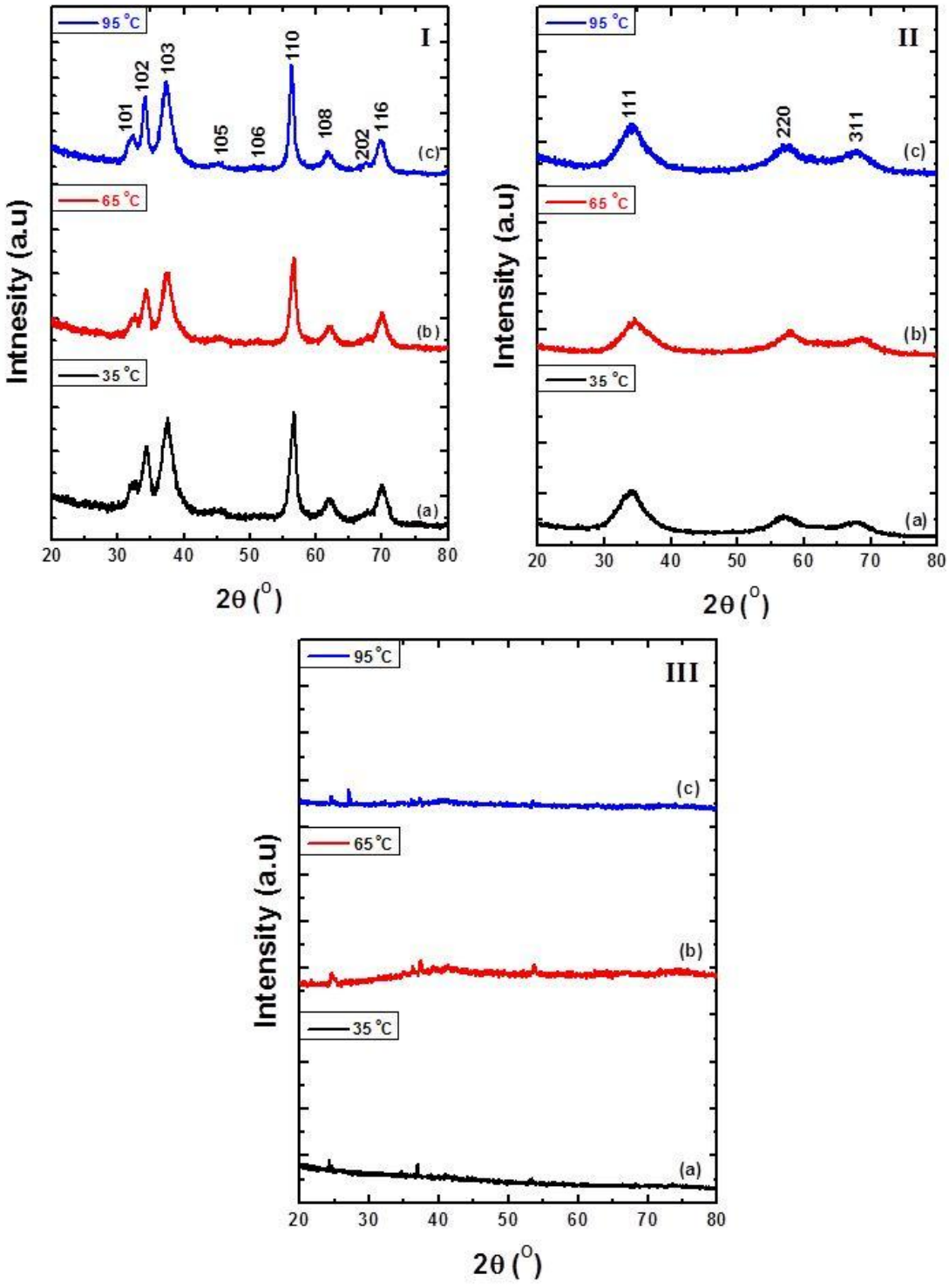

Figure 3.10. XRD patterns of L-aspartic acid-capped (I) CuS, (II) ZnS and (III) FeS nanoparticles synthesized at (a) 35 °C, (b) 65 °C and (c) 95 °C.

Fig. 3.11 shows the TEM images of prepared CuS, ZnS and FeS nanoparticles synthesized at different temperatures, i.e., 35, 65 and 95 ^{o}C. The particles obtained for CuS (Fig. 3.11(I)) had mixed morphology for all three set of temperature, i.e., rod-shaped, irregular-shaped nanoparticles, and hexagonal-shaped particles. At temperatures of 35 ^{o}C (Fig 3.11 I(a)) and 65 ^{o}C (Fig 3.11 I(b)), rod-shaped particles were dominating, whereas hexagonal-shaped particles dominated at a temperature of 95 ^{o}C.

As the temperature increases, the reaction approaches a critical temperature where almost one type of morphology is preferred. An increase in temperature, there is an increase in the average kinetic energy of the system. This causes the non-preferential morphology to destabilize, leaving only the stable particles. ZnS nanoparticles (Fig. 3.11 (II)) images show almost spherical-shaped particles for all three sets of temperature. However, as the temperature was increased, aggregation of nanoparticles was evident. The aggregation was attributed to the fact that the particles were very small and that the carboxylic acid group of the L-aspartic acid molecule is dehydrogenized more easily at pH 10 making the surface to become highly charged and resulting in the clustering of the nanoparticles.

Fig 3.11 (III) shows the TEM images of FeS nanoparticles synthesized at different temperatures, i.e., 35, 65 and 95 ^{o}C. Small spherical-shaped nanoparticles (Fig 3.11 (III a, b and c)) for all three sets of temperatures were observed. No significant change was observed as the temperature was increased.

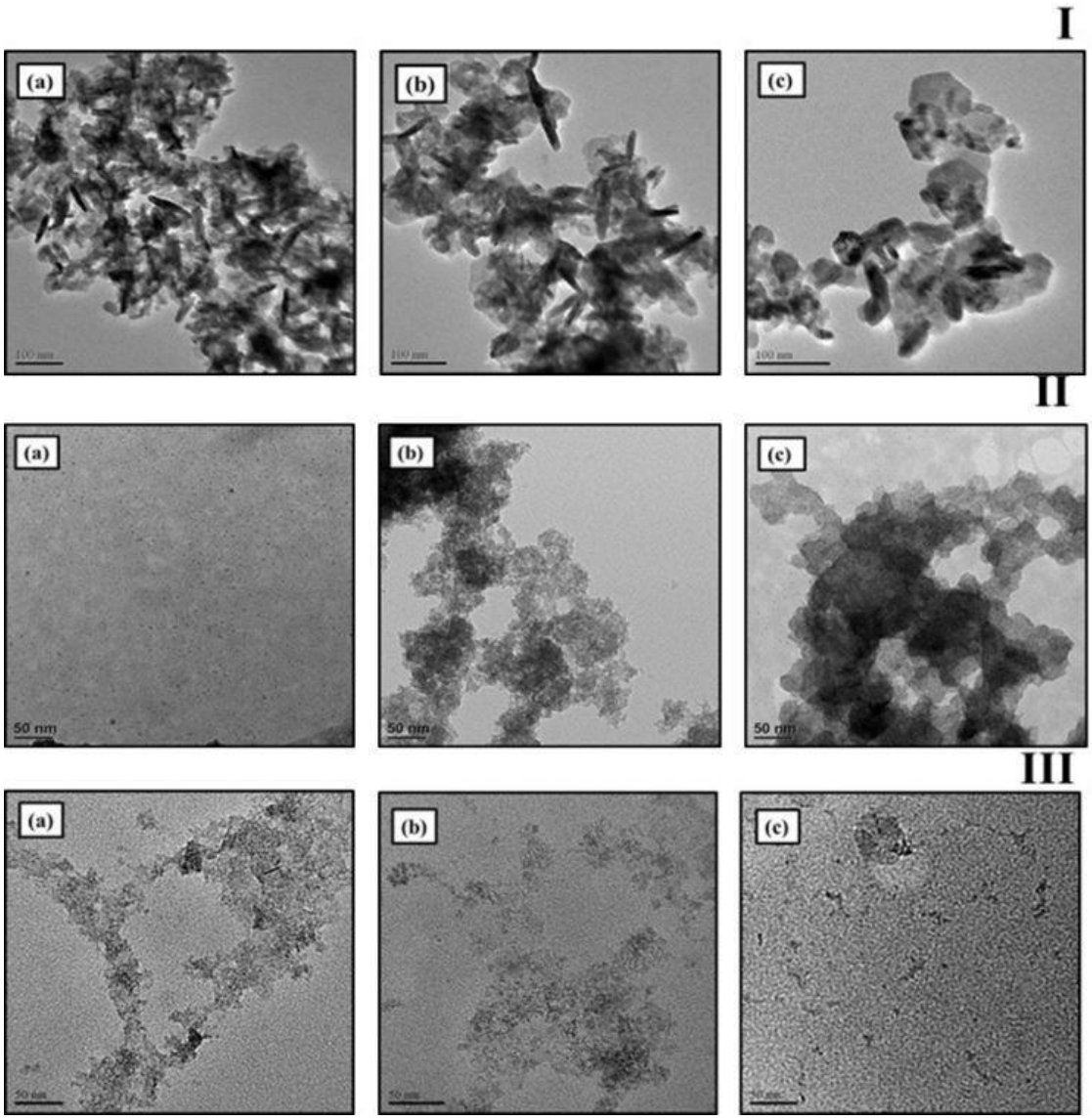

Figure 3.11. TEM images of L-aspartic acid-capped (I) CuS, (II) ZnS and (III) FeS nanoparticles synthesized at (a) 35 °C, (b) 65 °C and (c) 95 °C.

Fig. 3.12 (I-III) show the solubility test of L-aspartic acid-capped CuS, ZnS and FeS nanoparticles. The solubility increased with an increase in synthesis temperature for all CuS and ZnS nanoparticles. This result due to that as the temperature was increased the crystallinity of the particles also increase as seen in XRD peaks becoming sharper and visible with an increase in temperature. However for FeS nanoparticles all the samples show almost the same degree of solubility. This could be due to that the samples had almost equal particle

size and they were amorphous. At 95 °C, most of the particles were soluble in water for CuS and ZnS; this indicates that at this temperature the capping agent bind strongly to the surface of the nanoparticles.

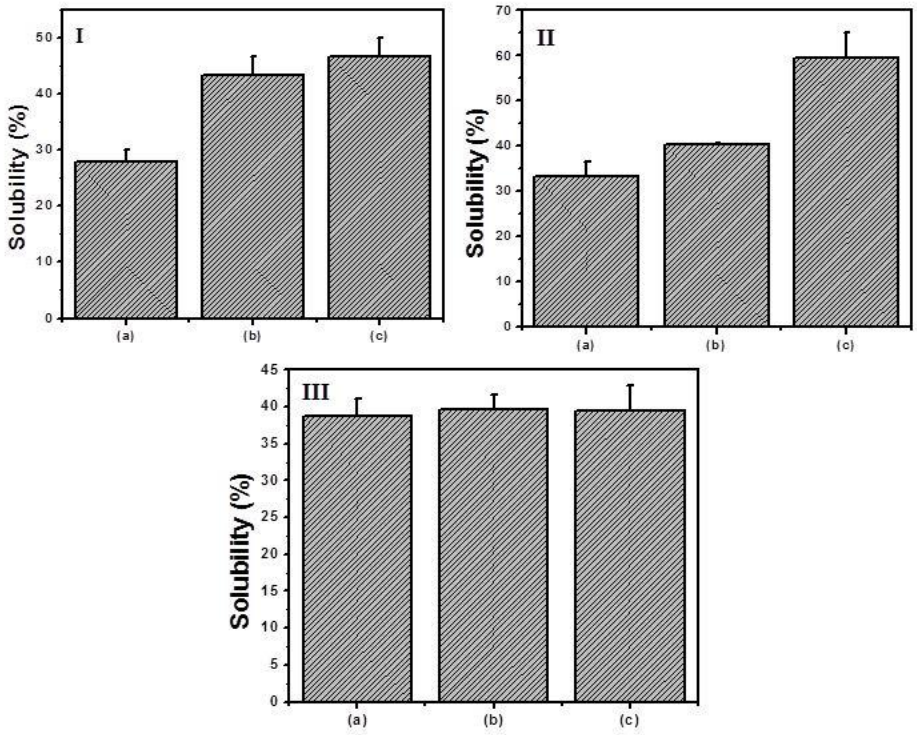

Figure 3.12. Water solubility graph of L-aspartic acid-capped (I) CuS, (II) ZnS and (III) FeS nanoparticles synthesized at 35 °C (a), 65 °C (b) and 95 °C (c).

3.2.3 *Lactose as capping agent for CuS, ZnS and FeS nanoparticles*

Lactose is the most important carbohydrate of the milk of most species and its biosynthesis takes place in the mammary gland. Concentrations of this compound in milk vary strongly with species. Lactose is the first and only carbohydrate every newborn mammal (including human) consumes in significant amounts. Lactose is a carbohydrate and as such a disaccharide. One molecule of lactose is built from one molecule each of two other carbohydrates, galactose, and glucose. The galactose and glucose moieties are linked together through a beta-(1, 4) glucosidic linkage. Lactose has hydroxyl active groups, which

can interact with the surface of the nanoparticles during preparation and again work towards improving the solubility of the particles in the aqueous environment.

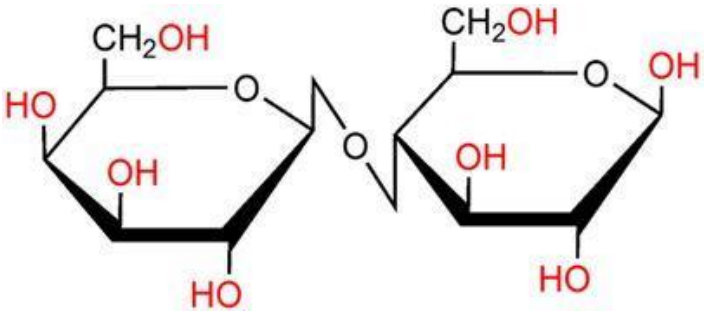

Scheme 3.4. Chemical structure of β-Lactose.

3.2.3.1 Interaction between Lactose and nanoparticles

The FTIR spectra (Fig. 3.13) were recorded in order to study the interaction of lactose molecules with the surface of CuS, ZnS and FeS nanoparticles. In Fig. 3.13(a) pristine lactose show two bands in the regions of 3100-3400 cm^{-1}, emanating from the O-H group that is bonded to the ring carbon. One band around 3527 cm^{-1} disappears when lactose is bonded to the surface of the nanoparticles. The spectra for all nanoparticles show a broad band at 3268 cm^{-1} which can be attributed to adsorption of H_2O. The other difference observed is that all nanoparticles (Fig. 3.13(b-d)) showed broad O-H and C-O stretch when compared to that of pristine lactose. Upon interaction with the nanoparticles, the metal sulfide draws the electron density towards itself resulting in the weakening of the other bonds and thus their shifts and broadness in the spectra.

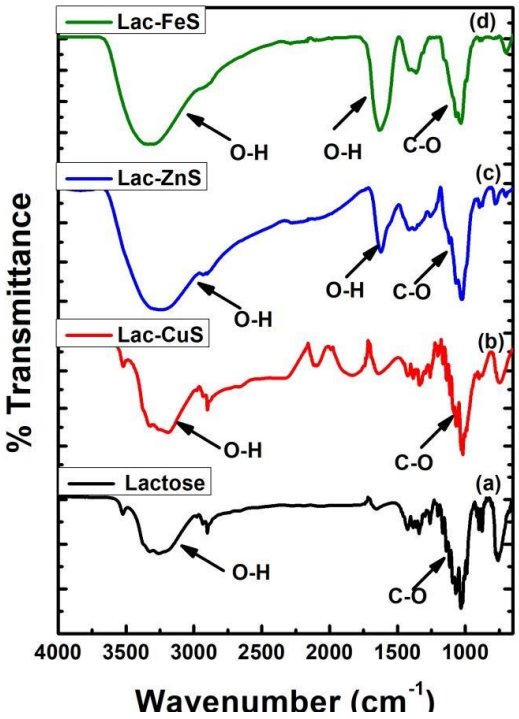

Figure 3.13. Infrared spectra of (a) pristine lactose, lactose-capped (b) CuS, (c) ZnS and (d) FeS nanoparticles.

3.2.3.2 Ultraviolet-visible and Photoluminescence spectroscopic characterization of nanoparticles

The optical properties of lactose-capped nanoparticles were investigated using UV-Vis absorption and photoluminescence spectroscopy. The absorption spectra of synthesized CuS, ZnS and FeS nanoparticles synthesized at different temperatures are shown in Fig. 3.14. All the absorption spectra were blue-shifted from their bulk counterparts due to quantum confinement effects. The optical properties of copper sulfide are rather fascinating; each stable phase displays its own characteristic properties, for example, covellite CuS has a distinctive absorption peak in the near infra-red region at approximately 920 nm and this value decreases as the sulfur content increases from covellite to digenite ($Cu_{1.8}S$) to djurleite ($Cu_{1.96}S$) (Haram *et al*. 1996). The graph in (Fig. 3.14(I)) shows absorption spectra of the as-prepared copper sulfide nanocrystals synthesized at 35, 65 and 95 ℃. The samples absorb in

the spectral region between 350–605 nm. In addition, a broad band extending into the near-IR region can be observed, which is characteristic for covellite CuS.

From the UV-Vis spectra of zinc sulfide nanoparticles (Fig. 3.14(II)), it shows that for the lowest synthetic temperature (Fig. 3.14(II)a), similar kind of an excitonic peak around 262 nm is observed as for the previous case of alanine-capped ZnS nanoparticles, indicating the presence of the $1S_e$-$1S_h$ excitonic transition in the ZnS nanoparticles. In addition, there is a sharp absorption shoulder around 340 nm for all samples, which is at a shorter wavelength than 345 nm of the bulk ZnS. Fig. 3.14(III) show the absorption spectra of iron sulfide nanoparticles. As seen in the spectra, the samples absorb in the spectral region between 300–400 nm.

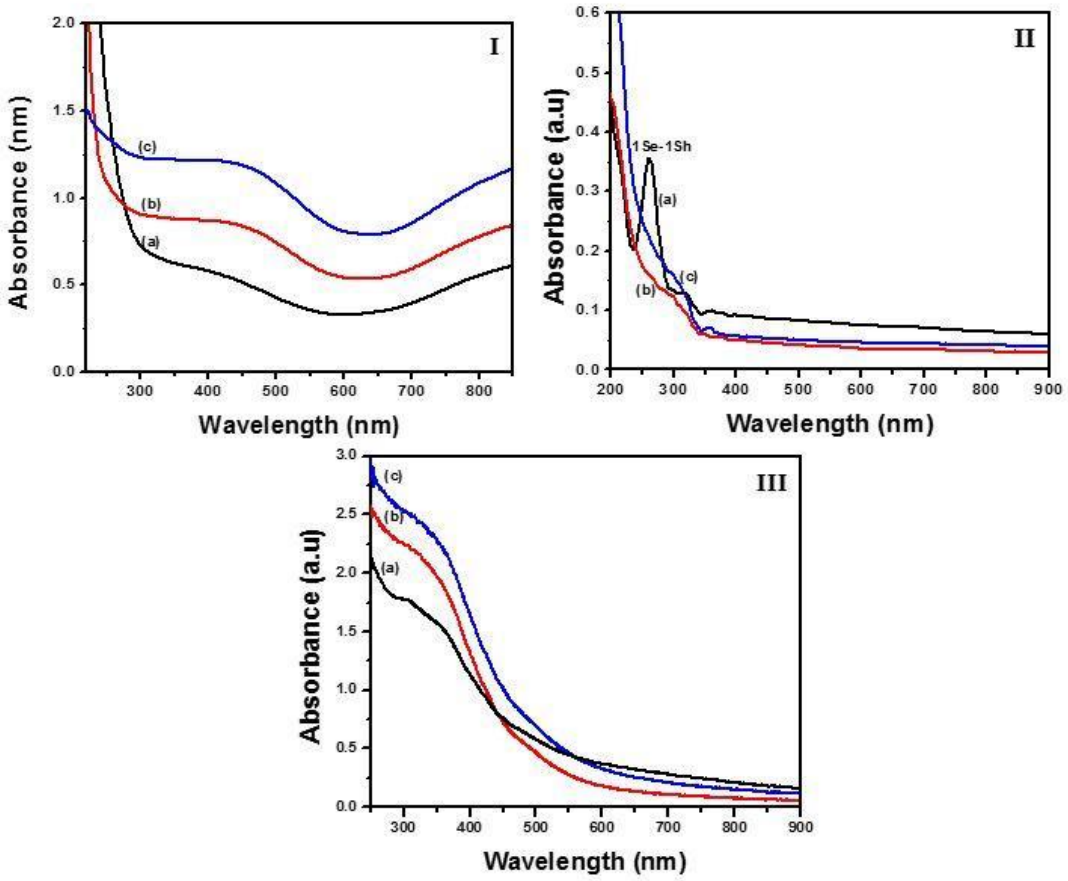

Figure 3.14. UV–Vis absorption spectra of lactose-capped (I) CuS, (II) ZnS and (III) FeS nanoparticles synthesized at (a) 35 °C, (b) 65 °C and (c) 95 °C.

In addition, the peaks had a higher degree tailing which might suggest that the particles are polydispersed. Table 3.6 show the optical data for all samples. The blue-shift for all samples suggest that the particles are very small and will, therefore, experience stronger confinement effects. As the reaction temperature was increased there was a successive red-shift as observed from the previously reported results.

Table 3.6. Band edges of lactose-capped CuS, ZnS and FeS nanoparticles synthesised at different temperatures.

Temperature (°C)	Band edges (nm)		
	CuS	ZnS	FeS
35	556	331	-
65	576	339	-
95	591	341	-

Photoluminescence spectra of samples at room temperature are shown in Fig. 3.15. Under the excitation of 275 nm, copper sulfide samples (Fig. 3.15(I)) showed narrow emission peak at ≈400 nm. The spectra also depicts relatively monodispersed nanocrystals, indicated by the Gaussian shaped curves and the narrowness of the curves. In addition the position of peaks remains virtually unaltered, although, the peak intensity for nanoparticles was different. This could be due to change in the size effect of the products, which results due to different preparation temperature. Fig. 3.15(II) and (III) is the emission spectra of ZnS and FeS nanoparticles excited at 300 nm. The position of peaks virtually altered with an increase in reaction temperature, signifying different properties. In addition, the spectra became broader as the temperature increased, signifying formation of bigger particle sizes and polydispersity.

This corroborates well with the results obtained in the absorption spectra where the band edge increased with increase in temperature.

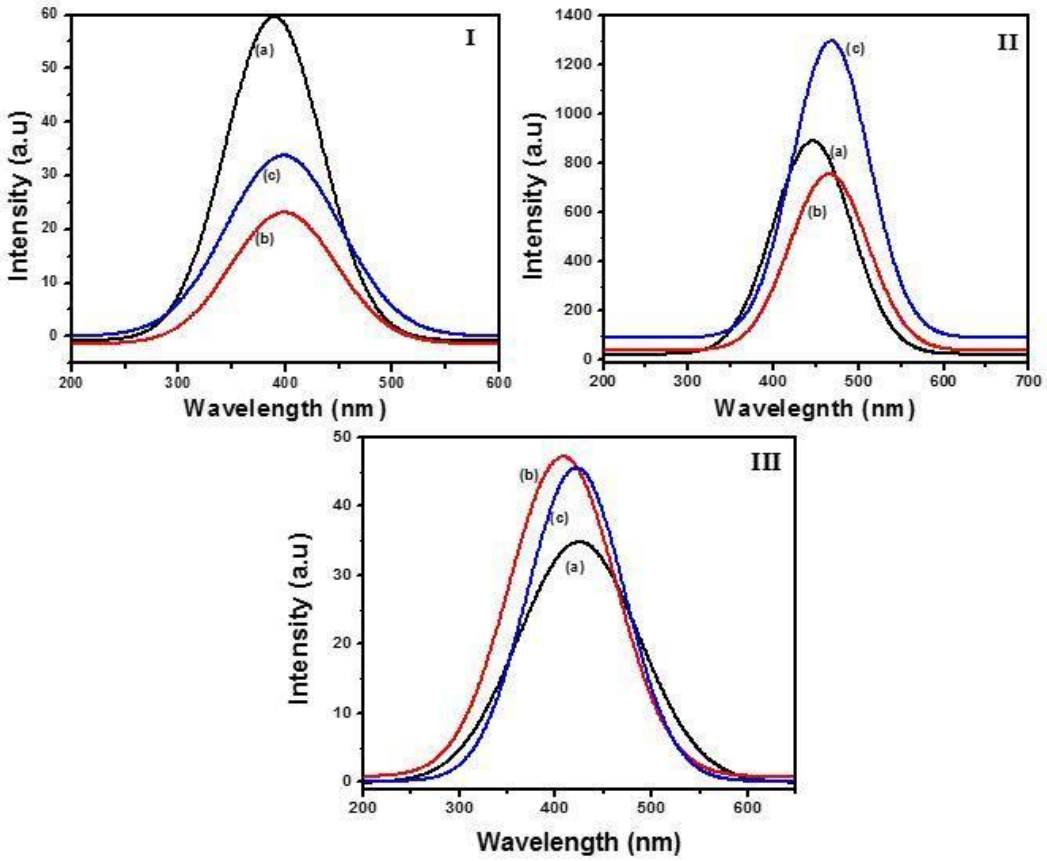

Figure 3.15. Photoluminescence spectra of lactose-capped (I) CuS, (II) ZnS and (III) FeS nanoparticles synthesized at (a) 35 °C, (b) 65 °C and (c) 95 °C.

Table 3.7. Emission maxima of synthesized CuS, ZnS and FeS nanoparticles at different temperatures.

Temperature (°C)	Emission maxima (nm)		
	CuS	ZnS	FeS
35	390	446	423
65	398	467	408
95	398	468	421

3.2.4.2 Structural properties

The XRD patterns of lactose-capped CuS, ZnS and FeS nanoparticles synthesized at 35, 65 and 95 °C are shown in Fig. 3.16. Fig. 3.16(I) shows the XRD pattern of CuS nanoparticles. The XRD data shows similar kind of peaks as for the previous case indicating the presence of covellite CuS phase. However, as the temperature was increased there was a disappearance of the (101) peak for the highest reaction temperature. The disappearance of the peak is believed to be due to change in morphology due to relatively high pressure generated during the high reaction temperature (95 °C).

Fig. 3.16(II) shows the diffraction peaks for ZnS nanoparticles. Same as CuS nanoparticles, ZnS XRD data shows similar kind of peaks as for the previous cases for alanine and aspartic acid, indicating the presence of blend ZnS phase. For both CuS and ZnS samples, no evidence of impurities was observed. However, for FeS nanoparticles (Fig. 3.16(III)), the diffraction peaks were less intense depicting close to amorphous nature of the products. This amorphous nature was attributed to the different reaction temperature used in their

preparation. The samples were closely indexed to the cubic greigite (Fe_3S_4) (ICDD No: 00-016-0713), with some impurities believed to result from the capping agent. Overall the increase in reaction temperature resulted in an increase in the intensity of peaks, indicating the formation of a highly crystalline product at a higher temperature. In addition, the narrowness of the peaks with an increase in reaction temperature was attributed to Oswald ripening.

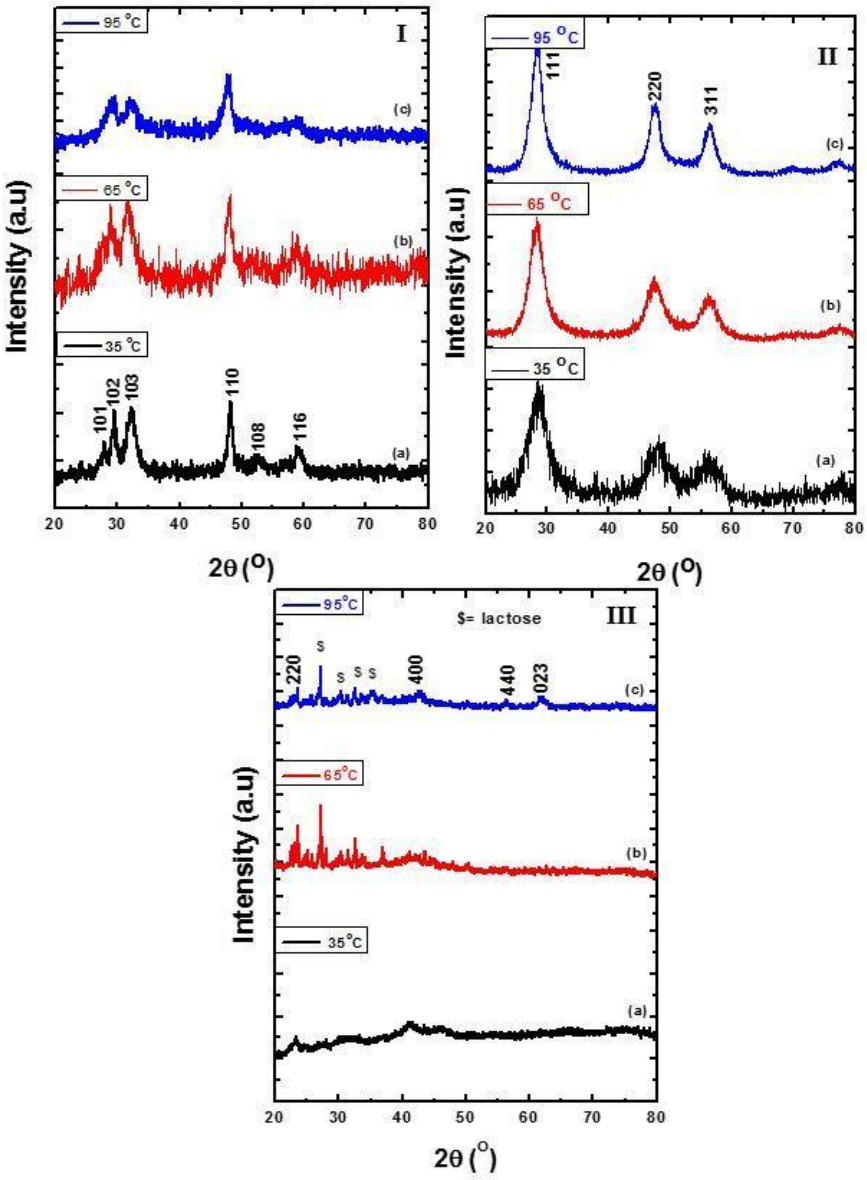

Figure 3.16. XRD patterns of lactose-capped (I) CuS, (II) ZnS and (III) FeS nanoparticles synthesized at (a) 35 °C, (b) 65 °C and (c) 95 °C.

Fig. 3.17 shows the morphologies of CuS, ZnS and FeS nanoparticles synthesized under different reaction temperature. As seen in Fig. 3.17(I) the CuS particles obtained for all three set of temperature had mixed morphology, i.e., rod-shaped and irregular-shaped nanoparticles, with rod-shaped particles dominating. As the temperature was increased the particles aggregated and formed nanoclusters. This change in morphology corroborates with the XRD data. The images which are shown in Fig. 3.17(II), represent the lactose-capped ZnS nanoparticles. It can be seen from the TEM images that the particles are close to spherical in shape with some degree of aggregation in chain-like form.

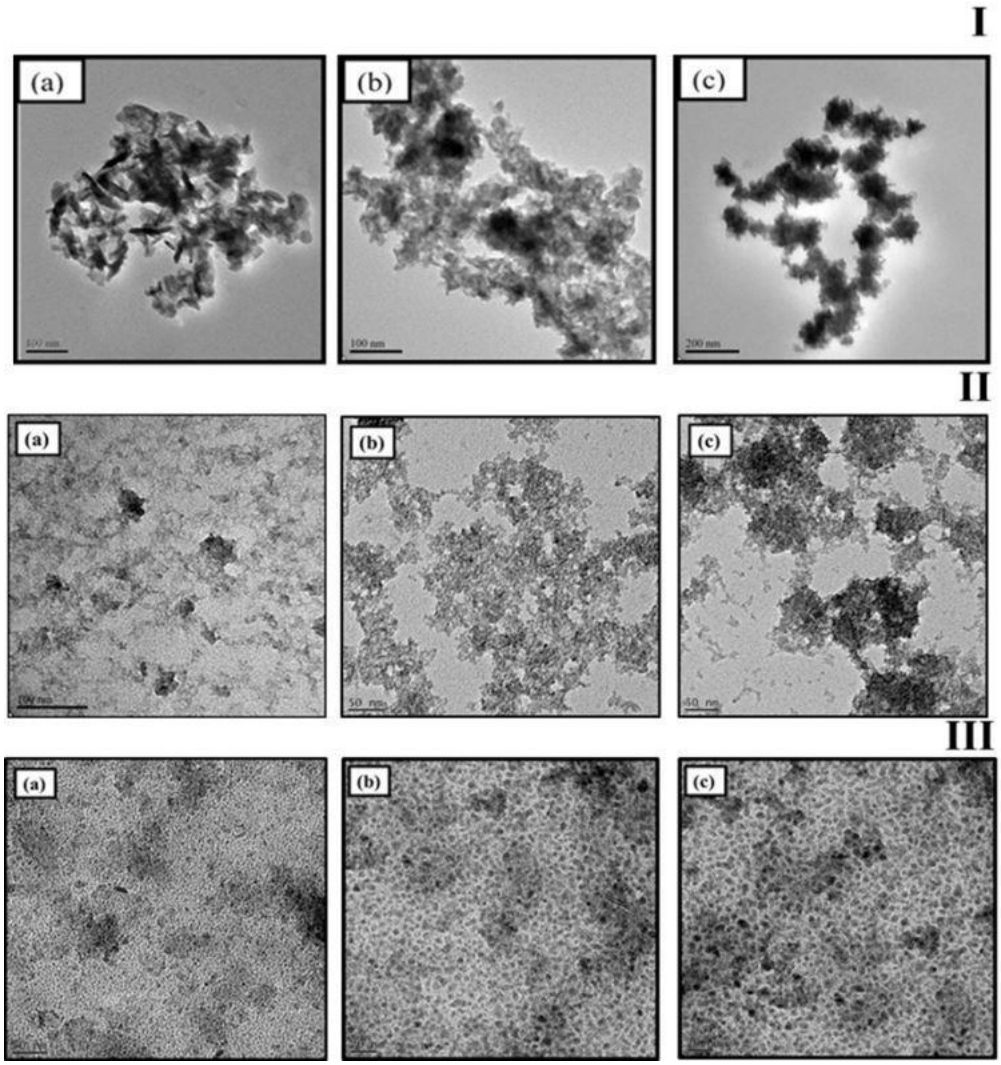

Figure 3.17. TEM images of lactose-capped (I) CuS, (II) ZnS and (III) FeS nanoparticles synthesized at 35 °C (a), 65 °C (b) and 95 °C (c).

The particles were too small and hence it was difficult to estimate their sizes. Fig. 3.17(III) shows the images of lactose-capped FeS nanoparticles. It is apparent that the products are composed of spherical-shaped FeS nanoparticles. The average particles size estimated from the images were found to be 3.76, 3.99 and 5.22 nm for sample synthesized at 35, 65 and 95 ^{o}C, respectively. As the temperature was increased the morphology of the particles did not change, however, the particles size increased. The particle size increase with an increase in synthesis temperature was attributed to Oswald repining.

Fig. 3.18 (I-III) shows the solubility test of lactose-capped CuS, ZnS and FeS nanoparticles. The solubility of CuS and FeS nanoparticles increased with an increase in synthesis temperature. This could be due to that at high temperature the capping agent bind strongly to the surface of the nanoparticles.

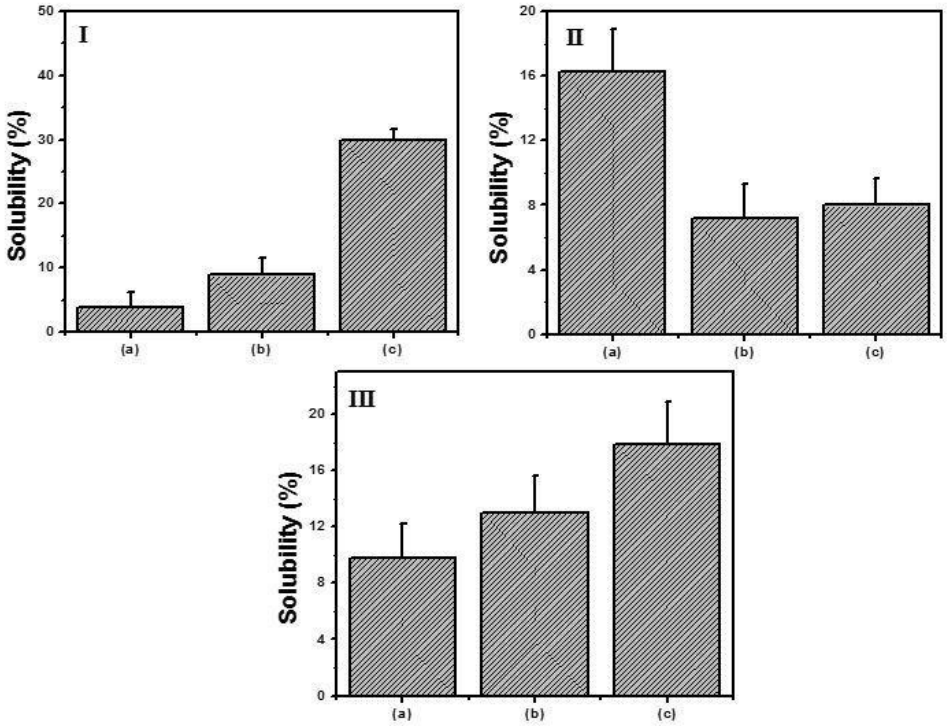

Figure 3.18. Water solubility graph of lactose-capped (I) CuS, (II) ZnS and (III) FeS nanoparticles synthesized at 35 °C (a), 65 °C (b) and 95 °C (c).

As seen in optical and TEM results, the particles were aggregated and approached uniformity with increase in temperature. On the other hand, the solubility test for lactose-capped ZnS nanoparticles (Fig. 18(II)) showed no direct relationship between solubility and temperature increase. The nanoparticles synthesized at 35 °C were more soluble as compared to those synthesized at higher temperatures.

3.3 Conclusion

Metal sulfide nanoparticles have been synthesized by the aqueous medium through a simple colloidal route. The use of alanine, aspartic acid and lactose as a capping agents and the synthetic temperature are important parameters that determined the final morphology and size of the nanoparticles. These parameters had an effect on both the optical and morphological properties of the nanoparticles. The growth in size with temperature was attributed Ostwald ripening effects whilst the change in morphology was associated to thermodynamic growth regime.

The optical properties of all the metal sulfide nanoparticles showed amazing results, with very large blue-shifts in band gap observed. These large blue-shifts were associated with various factors such as the size, shape and phase of nanocrystals. Even though the absorption spectra were blue shifted from their bulk materials, most of their photoluminescence spectra were very broad signifying that the particles were not well passivated. The XRD patterns confirmed that the type of the capping agents used in this study had little or no significant effect on the composition of the nanoparticles as there was only one phase observed for CuS and ZnS nanoparticles as the type of the capping agent was varied.

The TEM images also confirmed the size and the shape of the nanoparticles. Different morphologies were observed, from rod-shaped CuS to close to spherical ZnS and FeS. In addition the size of some particles were not measure due to change in morphology and very

small sizes. For L-alanine-capped CuS, ZnS and FeS nanoparticles the highest synthesis temperature (95 °C) resulted in particles with properties superior to the ones synthesized at lower temperatures and the surface coverage of the nanoparticles with L-alanine improved with increasing temperature evident from the degree of water solubility of the nanoparticles. However for L-aspartic acid and lactose capped nanoparticles there was no consistency in terms of the effect of synthesis temperature on the degree of solubility. Overall, this method works better for the preparation of CuS and ZnS than FeS nanoparticles.

3.4 References

AHMAD, A., MUKHERJEE, P., MANDAL, D., SENAPATI, S., KHAN, M.I., KUMAR, R., and SASTRY, M., 2002. Enzyme mediated extracellular synthesis of CdS nanoparticles by the fungus, Fusarium oxysporum. *Journal of American Chemistrey Scociety*, **124**, 12108–12109.

AKHTAR, M., and O'BRIEN, P.P., 2013. Synthesis of iron chalcogenide nanocrystals and deposition of thin films from single source precursors. *School of Chemistry*, Ph.D. Thesis.

ALAM, M.J. and AHMAD, S., 2012. Anharmonic vibrational studies of L-aspartic acid using HF and DFT calculations. *Spectrochimica Acta Part A: Molecular and Biomolecular Spectroscopy*, **96**, 992–1004.

BARNHAM, K., MARQUES, J.L., HASSARD, J., and O'BRIEN, P., 2000. Quantum-dot concentrator and thermodynamic model for the global redshift. *Applied Physics Letters*, **76**, 1197–1199.

BRUCHEZ, M., MORONNE, M., GIN, P., WEISS, S., and ALIVISATOS, A.P., 1998.

Semiconductor nanocrystals as fluorescent biological labels. *Science*, **281**, 2013–2016.

CHAN, W.C., and NIE, S., 1998. Quantum dot bioconjugates for ultrasensitive nonisotopic detection. *Science*, **281**, 2016–2018.

GAO, M., LESSER, C., KIRSTEIN, S., and MOHWALD, H., 2000. Electroluminescence of different colors from polycation/CdTe nanocrystal self-assembled films. J*ournal of Applied Physics*, **87**, 2297–2302.

HARAM, S.K., MAHADESHWAR, A.R., and DIXIT, S.G., 1996. Synthesis and characterization of copper sulfide nanoparticles in Triton-X 100 water-in-oil microemulsions, *Journal of Physical Chemistry*, **100**, 5868–5873.

HEO, J., and HWANG, C., 2016. Application of L-aspartic acid-capped ZnS : Mn colloidal nanocrystals as a photosensor for the detection of copper (II) ions in aqueous solution. *Nanomaterials*, **6**, 82.

LEE, S., KIM, K., and HWANG, C., 2009. Syntheses and characterizations of valine and alanine capped water soluble ZnS nanoparticles. *Journal of the Korean Chemical Society*, **53**, 505–511.

LAI, Y., YIN, W., and LIU, J., 2010. One-pot green synthesis and bioapplication of L-arginine-capped superparamagnetic Fe_3O_4 nanoparticles. *Nanoscale Research Letters*, **5**, 302–307.

MURPHY, C.J., 2002. Optical sensing with quantum dots. *Analytical Chemistry*, **74**, 521A–526A.

NELWAMONDO, S.M.M., MOLOTO, M.J., KRAUSE, R.W.M., and MOLOTO, N., 2012. Synthesis and characterization of alanine-capped water soluble copper sulphide

quantum dots. *Materials Letters*, **75**, 161–164.

OLUWAFEMI, S.O., REVAPRASADU, N., and RAMIREZ, A.J., 2008. A novel one-pot route for the synthesis of water-soluble cadmium selenide nanoparticles. *Journal of Crystal Growth*, **310**, 3230–3234.

OTHMAN, A.A., OSMAN, M.A., and WAHDAN, M.H., 2014. Thermal annealing and UV induced effects on the structural and optical properties of capping free ZnS nanoparticles synthesized by co-precipitation method. *International Journal of General Engineering and Technology*, **3**, 9–16.

PEREIRO, R., COSTA-FERNANDEZ, J.M., and SANZ-MEDEL, A., 2006. The use of luminescent quantum dots for optical sensing. *Trends in Analytical Chemistry*, **25**, 207–218.

RAJKUMAR, B.J.M., RAMAKRISHNAN, V., and RAJARAM, R.K., 1998. Infrared and Raman spectra of DL-aspartic acid nitrate monohydrate. *Spectrochimica Acta Part A*, **54**, 1527–1532.

ROY, P., and SRIVASTAVA, S.K., 2007. Low-temperature synthesis of CuS nanorods by simple wet chemical method. *Materials Letters*, **61**, 1693–1697.

SARANYA, M., SANTHOSH, C., RAMACHANDRAN, R., and GRACE, A.N., 2014. Hydrothermal growth of CuS nanostructures and its photocatalytic properties. *Powder Technology*, **252**, 25–32.

SIBIYA, P.N., XABA, T., and MOLOTO, M.J., 2016. Green synthetic approach for starch capped silver nanoparticles and their antibacterial activity. *Pure Applied Chemistry*, **88**, 1–9.

SUTHERLAND, A.J., 2002. Quantum dots as luminescent probes in biological systems.

Current Opinion in Solid State and Materials Science, **6**, 365–370.

TAN, C., ZHUB, Y., LUA, R., XUEA, P., BAOA, C., LIUA, X., FEIA, Z., and ZHAO, Y., 2005. Synthesis of copper sulfide nanotube in the hydrogel system. *Materials Chemistry and Physics*, **91**, 44–47.

WANG, L., TAO, X., YANG, J., REN, Y., LIU, Z., and JIANG, M., 2006. Preparation and characterization of the ZnS nanospheres with narrow size distribution. *Optical Materials*, **28**, 1080–1083.

WANG, S., MAMEDOVA, N., KOTOV, N.A., CHEN,W., and STUDER, J., 2002. Antigen/antibody immunocomplex from CdTe nanoparticle bioconjugates. *Nano Letters*, **2**, 817–822.

Chapter 4

Biological evaluation of alanine capped nanoparticles

3.1 Introduction

Nowadays nanotechnology has remodelled the technology progress and it is believed to be one of the key technologies of the 21st century (Wagner *et al*. 2011). A wide variety of nanomaterials have attracted tremendous attention from researchers, because of their unique properties which can be quite different from those exhibited in the bulk state. Many properties are found to change in the nanoscale, for example, physical characteristics, surface area, magnetic, mechanical, optical as well as chemical properties such as reactivity and thermal properties. Hence these materials are increasingly being used in the commercial manufacture of fillers, catalysts, semiconductors, cosmetics, microelectronics, and drug carriers (Srivatsan 2011).

It is projected that in the next few coming years the production of nanoparticles will increase from the estimated 2 300 tons produced in the last decade to 58 000 tons by 2020 (Maynard 2006). With this increase in manufacturing of nanoparticle-containing materials along with the constant discovery of new applications of nanoparticles, it is alarming that knowledge on the health effects of nanoparticles exposure is still limited. However, the number of efforts aimed at determining the health risks associated with nanoparticle are surfacing but at a slow rate (see review by Lewinski (Lewinski *et al*. 2008)). Thus, with this advancement in synthesis and applications of nanomaterials, researchers need to focus more on the cytotoxicity of nanomaterials in order to try to limit their health risks.

In recent days much effort has been directed in the search for new antibacterial agents to fight against the continuing developing resistivity of bacteria towards strong antibiotics

(Borkow & Gabbay 2004). It is now well recognized that inorganic materials can destroy bacteria, without toxicating the surrounding tissues (Rubilar et al. 2013; Kumar *et al*. 2013; Arulmurugan *et al*. 2010). Metals like silver, copper, gold, titanium, and zinc have been used for centuries as bactericidal agents due to each having different properties and spectra of activity (Elghanian *et al*. 2012). The antibacterial, antifungal, and antiviral actions of sulfide nanoparticles have been broadly investigated in comparison with other metals (Wadhwani & Jain 2015).

However, the possible antimicrobial activity of copper sulphide nanoparticles is not yet explored, although it can act as an efficient radiotracer for pharmacokinetics, biodistribution, and positron emission tomography (Zhou *et al*. 2010). Chakraborty and co-workers examined the antibactericidal activity of copper sulfide nanoparticles against five bacterial species (viz., *Bacillus subtilis*, *Listeria monocytogens*, *E. coli*, *Pseudomonas fluorescens* and *Salmonella typhimurium*) and five fungal species (viz., *Mucor*, *Rhizopus*, *Fusarium oxysporum*, *Alternaria* and *Helminthosporium*). The antimicrobial and antifungal activities of CuS nanoparticles were found to depend largely on the morphology of the nanoparticles. On another study (Ghaedi *et al*. 2016) tested the antibacterial and antifungal properties of CuS nanoparticles combined with root and shoot extracts from *L. usitatissimum*. The samples were screened against one type of Gram-positive and three Gram-negative bacteria: *S. aureus*, *A. Baumannii*, and *A. oryzae* fungal, using agar well diffusion method and comparing their antibacterial activities with the antibiotics *Gentamicin, Cephalexin,* and *Amphotericin B*. The information obtained from the MIC and MBC of both samples showed that plant capped CuS nanoparticles have more antibacterial and antifungal effects than the normal CuS nanoparticles. Thus the use of metal nanoparticles with plant extracts in sensitive environments, such as hospital, was suggested. However, before application of nanoparticles into the biological system, cytotoxicity tests are ideal.

The possibilities of the uptake of nanoparticles into the human body are reported to be mainly via the skin, respiratory tract, or the gastrointestinal tract (Wagner *et al*. 2011). Therefore, nanoparticle size, shape, and surface modification play an important role in the distribution in the organism. Nanoparticles absorbed via the respiratory tract can reach the lymph stream and the blood circulation (Hussain *et al*. 2001). Other groups have reported that nanoparticles are able to pass through the blood-brain-barrier (Kim *et al*. 2006) and through cell membranes (Foley *et al*. 2002) and can thus deposit in organs and interact with biological systems.

In addition some constituents of semiconductor nanoparticles such as copper ions (Rubilar *et al*. 2013) are toxic to many cells and hence harmful effects can be expected, especially when the hydrophilic capping agent or ligand around the nanoparticles is not stable and might dissolve and hence release toxic ions. Therefore, in this chapter, toxicity of L-alanine-capped CuS nanoparticles and as well as their antimicrobial activity were investigated. Different conditions such as concentration and time were considered. Application of nanomaterials as antimicrobial agents requires toxicity tests to be investigated to understand fully the behavioural response of the cells to the specified nanoparticles.

3.2 Results and discussion

3.2.1 Cytotoxicity and antimicrobial activity of alanine capped CuS nanoparticles

Because copper sulfide nanoparticles are used in many application fields and previous studies showed the possible hazardous effects of these materials it is important to investigate the toxic action more intensely. Therefore, *in vitro* cellular uptake experiments were performed to investigate the toxic effect of copper sulfide nanoparticles on human cervical carcinoma cells (HeLa). The viability of the cells cultivated in the presence of different

concentrations of CuS nanoparticles and was measured employing the MTS assay, a well-established method to determine the viability of mammalian cells. Furthermore the nanoparticles were assessed for their antibacterial properties against different strains of bacteria and fungi.

Fig. 4.1 and 4.2 shows the viability of HeLa cells treated with various concentrations of nanoparticles, determined via the MTS assay. Gold nanoparticles were used as a control in our experiments as they are known to be less toxic. The basic principal of this assay is that viable cells are able to reduce the MTS tetrazolium compound to produce a coloured formazan product that can be measured spectrophotometrically. Results from the assay show that the treatment of cells with CuS nanoparticles induced a concentration dependant toxicity profile whereby the toxicity increases with an increase in nanoparticle concentration. There is an increased cell viability observed at nanoparticle concentrations below 0.125 µg/ml, with the toxicity levels approaching that of gold nanoparticles which are known to be less toxic. According to Fig. 4.1 and 4.2, nanoparticles synthesized at 65 °C are less toxic compared to other temperatures (35 and 95 °C). The same trend for both experiments show the reliability of the results.

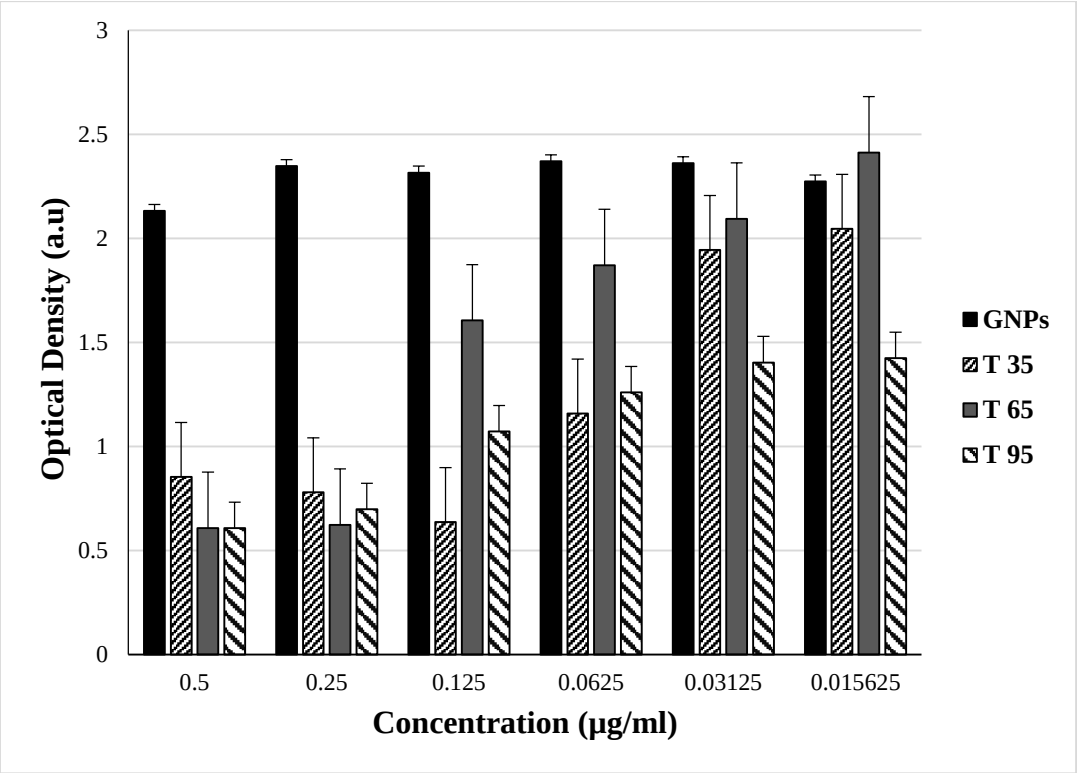

Figure 4.1. Bar graph of viability of HeLa cells treated for 24 hours at different concentrations.

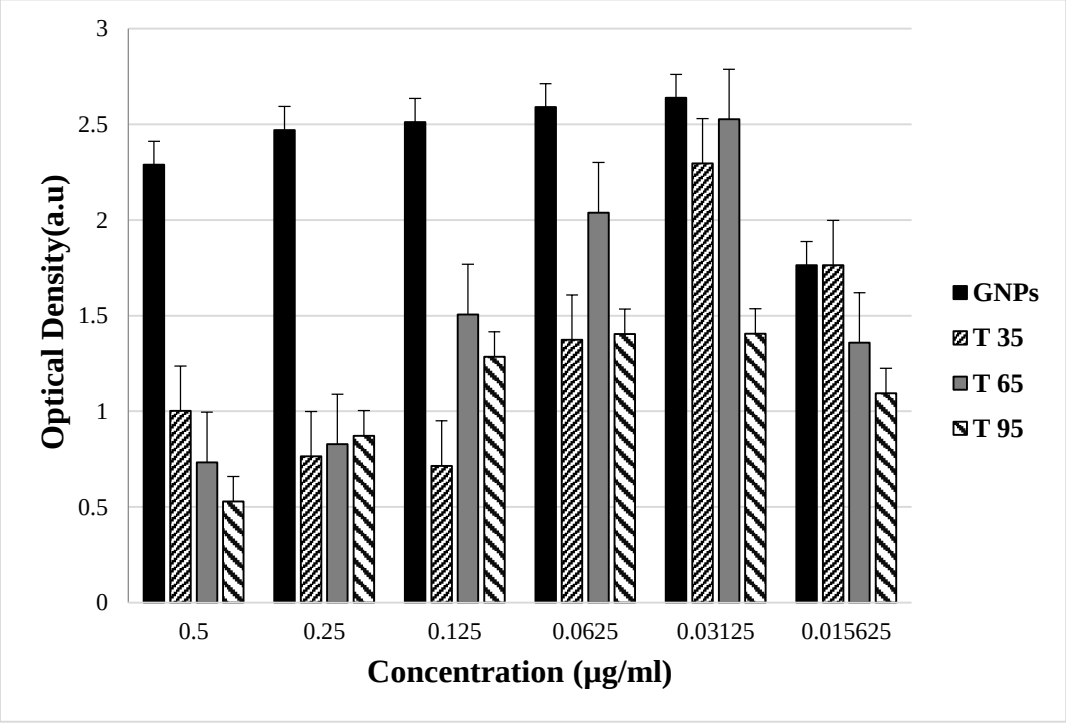

Figure 4.2. Bar graph of viability of HeLa cells treated for 24 hours at different concentrations.

Table 4.1 summarises the CC_{50} values calculated from the above experiments. The CC_{50} is the minimum concentration of nanoparticles that has achieved 50 % death of viable cells (Betancur-galvis *et al*. 2002). This table shows that nanoparticles synthesized at 95 were less toxic than all the other ones. This might be due to the fact that at this temperature the particles have a slightly bigger size compared to others, and hence did not cause much damage to the cells compared to the smaller nanoparticles which are able to penetrate the nucleus and induce cell death (Park *et al*. 2011).

Table 4.1. Minimum concentration of nanoparticles that has achieved 50 % death of viable cells.

Nanoparticles	1 CC_{50}	2 CC_{50}	Ave CC_{50}	STD Dev
CuS 35 °C	0.054	0.060	0.057	0.004
CuS 65 °C	0.130	0.110	0.120	0.014
CuS 95 °C	0.126	0.200	0.163	0.052

Table 4.2 show a comparative study of antimicrobial activity of uncapped CuS, Aln-capped CuS, uncapped ZnS and Aln-capped ZnS nanoparticles prepared at 35 °C. The antimicrobial activity results indicate that copper sulfide capped nanoparticles were more effective against the bacteria than zinc nanoparticles. In addition the uncapped CuS nanoparticles performed better than all the nanoparticles. This is due to the fact that in uncapped copper sulfide nanoparticles, Cu^{2+} ions leach out and penetrate the cell membrane resulting in the disruption of biochemical pathways through chelating cellular enzymes and DNA damage (Bogdanovi *et al*. 2014). *S. aureus* was the most susceptible microorganism with MIC of 0.05 mg/mL

for uncapped-CuS while *P. aeruginosa* and *C. neoformans* were the least susceptible with MIC of 3.125 mg/mL for both uncapped-CuS and Aln-CuS (see below Table 4.2).

In another study, Mandal and co-workers reported that *S. aureus* is the most susceptible micro-organism to zinc ferrite nanoparticles (Mandal *et al*. 2016). The capped copper nanoparticles seem to be more effective against gram positive compared to gram negative bacteria and fungi. This is attributed to the differences in the structure of their cell walls. The cell wall of gram negative bacteria is comprised of a thin peptidoglycan layer and an outer lipopolysaccharide layer whereas, the cell wall of gram positive bacteria is composed of a thick peptidoglycan layer but does not have the outer lipopolysaccharide.

Table 4.2. Minimum inhibitory concentration (MIC) of amino acid capped copper and zinc sulfide nanoparticles (mg/mL).

Bacterial strains	**Nanoparticles**			
	Copper		**Zinc**	
	Unc-CuS	Aln-CuS	Unc-ZnS	Aln-ZnS
S. aureus	< 0.05	0.10	0.20	3.13
E. faecalis	0.39	0.78	1.56	25.00
K.pnuemoniae	0.20	0.39	0.40	25.00
P.aeruginosa	3.13	1.56	0.78	0.78
C.albicans	1.56	1.56	0.20	6.25
C. neoformans	0.39	3.13	1.56	12.50

Neomycin MIC (ug/ml): *S.aureus:* <0.4*; E.faecalis:*6.25 *; K.pnuemoniae:* 12.5*; P.aeruginos:* <0.4.*; C.albicans:nd ; C. neoformans: nd*

3.3 Conclusion

The work done in this chapter shows that the particles were nontoxic at low to moderate concentrations and only induced toxicity at higher concentrations. Particles synthesized at 95 °C were less toxic compared to other nanoparticles (35 and 65 °C) for both two set of experiments, as informed by the CC_{50} values. However, since it is known that copper ions and materials that contain sulphur are toxic, various points need to be investigated before looking at biological applications. Those points include the duration or time frame of detecting the toxicity of nanoparticles, and the concentration of the nanoparticles.

Toxicity studies on ZnS nanoparticles were not done due to unsuccessful growth of cells. The antimicrobial properties were tested using different strains of both positive and negative bacteria and fungi. It was found that Aln-capped copper sulfide nanoparticles were more effective against the bacteria than Aln-capped zinc sulfide nanoparticles. *Staphylococcus aureus* (ATCC 25923) was the most susceptible with an MIC of 0.05 mg/mL for uncapped-CuS nanoparticles while *Pseudomonas aeruginosa* (ATCC 15442) and *Cryptococcus neoformans* (ATCC 14116) were the least with MIC of 3.125 mg/mL for both uncapped-CuS and Aln-capped CuS. Overall uncapped copper sulfide nanoparticles performed better than all the particles.

However before these particles can be used in biological applications more studies are needed which include critical nanoparticle characterization both prior to and after mixing with the biological media, with a focus on the change of the physical properties such as aggregation state, effective surface charge and desorption of chemicals from the surface of the nanoparticles.

3.4 References

ARULMURUGAN, S., KAVITHA, H.P., and VENKATRAMAN, B.R., 2010. Biological activities of schiff base and its complexes: A review. *Rasayan Journal of Chemistry*, **3**, 385–410.

BETANCUR-GALVIS, L.A., MORALES, G.E., FORERO, J.E., and ROLDAN, J., 2002. Cytotoxic and antiviral activities of Colombian medicinal plant extracts of the Euphorbia genus, *Memorias do Instituto Oswaldo Cruz*, **97**, 541–546.

BOGDANOVIC, U, LAZIC, V., VODNIK, V., BUDIMIR, M., and MARKOVIC, Z., 2014. Copper nanoparticles with high antimicrobial activity. *Materials letters*, **128**, 75–78.

BORKOW, G., and GABBAY, J., 2004. Putting copper into action : Copper-impregnated products with potent biocidal activities. *The FASEB Journal*, **18**, 1728–1730.

ELGHANIAN, R., STORHOFF, J.J., MUCIC, R.C., LETSINGER, R.L., and MIRKIN, C.A., 1997. Selective colorimetric detection of polynucleotides based on the distance-dependent optical properties of gold nanoparticles, *Science*, **277**, 1078.

FOLEY, S., CROWLEY, C., SMAIHI, M., BONFILS, C., ERLANGER, B.F., SETA, P and LARROQUE, C., 2002. Cellular localisation of a water-soluble fullerene derivative. *Biochemical and Biophysical Research Communications*, **294**, 116–119.

GHAEDI, M., YOUSEFI-NEJAD, M., SAFARPOOR, M., KHAFRI, H.Z., TYAGI, I., AGARWAL, S., and GUPTA, V.K., 2016. Synthesis of CuS nanoparticles and evaluation of its antimicrobial properties in combination with Linum usitatissimum root and shoot extract. *Desalination and Water Treatment*, **57**, 3994.

HUSSAIN, N., JAITLEY, V. and FLORENCE, A.T., 2001. Recent advances in the understanding of uptake of microparticulates across the gastrointestinal lymphatics.

Advanced Drug Delivery Reviews, **50**, 107–142.

KIM, J.S., YOON, T, YU, K.N., KIM, B.G., PARK,S.J., KIM, H.W., LEE, K.H., PARK,S.B., LEE, J and CHO, MH., 2006. Toxicity and tissue distribution of magnetic nanoparticles in mice, *Toxicological Sciences*, **89**, 338–347.

KUMAR, R., SHARMA, S., SINGH, R.V., and RASTOGI, S., 2013. Synthesis, Characterization and biological evaluation of niobium (v) complexes of coumarin based imines, *Rasayan Journal of Chemistry*, **6**, 183–189.

LEWINSKI, N., COLVIN, V., and DREZEK, R., 2008. Cytotoxicity of nanoparticles, *Small*, **4**, 26–49.

MANDAL, S., NATARAJAN, S., TAMILSELVI, A., and MAYADEVI, S., 2011. Photocatalytic and antimicrobial activities of zinc ferrite nanoparticles synthesize through soft chemical route: A magnetically recyclable catalyst for water/waste water. *Journal of Environmental Chemical Engineering*, **4**, 2706–2712.

MAYNARD, A.D., 2006. *Nanotechnology* : A Research Strategy for Addressing Risk. 1st ed. Washington, DC: Woodrow Wilson International Center for Scholars, Project on Emerging Nanotechnologies, Print.

PARK, M.V.D.Z., NEIGH, A.M., VERMEULEN, J.P., FONTEYNE, L.J.J., VERHAREN, H.W., BRIEDÉ, J.J., LOVEREN, H., and JONG, W.H., 2011. The effect of particle size on the cytotoxicity, inflammation, developmental toxicity and genotoxicity of silver nanoparticles, *Biomaterials*, **32**, 9810–9817.

PRABHU, B.M., ALI, S.F., MURDOCK, R.C., HUSSAIN, S.M., and SRIVATSAN, M., 2011. Copper nanoparticles exert size and concentration dependent toxicity on somatosensory neurons of rat, *Nanotoxicology*, **4**, 150–160.

RUBILAR, O., RAI, M., TORTELLA, G., DIEZ, M.C., SEABRA, A.B., and DURAN, N et al., 2013. Biogenic nanoparticles : copper , copper oxides , copper sulphides , complex copper nanostructures and their applications, *Biotechnology Letters,* **35**,1365–1375.

WADHWANI, M., and JAIN, S., 2015. Synthesis and antimicrobial activity of zinc sulphide nanoparticles, *Research Journal of Recent Sciences*, **4**, 36–39.

WAGNER, S., BLOH, J., KASPER, C., and BAHNEMANN, D., 2011. Toxicological issues of nanoparticles employed in photocatalysis. *Green*, **1**, 171–188.

ZHOU, M., ZHANG, R., HUANG, M., LU,W., SONG, S., MELANCON, M.P., TIAN, M., LIANG, D., and LI, C., 2010. A chelator-free multifunctional [^{64} Cu]-CuS nanoparticle platform for simultaneous micro-PET/CT imaging and photothermal ablation therapy. *Journal of the American Chemical Society*, **132**, 15351–15358.

Chapter 5

General conclusion and recommendations

The synthesis of water soluble semiconductor nanoparticles using colloidal aqueous synthesis route yielded faceted shaped particles ranging from rods, spheres and hexagonal, as determined by TEM. All absorption spectra were blue-shifted to their corresponding bulk, signifying finite sizes of the nanoparticles. The PL spectra were red-shifted for all samples except for CuS samples which were blue-shifted perhaps due to surface defects. In addition the broad peaks showed that the particles were polydispersed.

Three water soluble capping molecules, i.e., L-alanine, L-aspartic acid and lactose, were employed in the preparation of CuS, ZnS and FeS nanoparticles at different temperatures. The role of the above capping agents was to shape the nanoparticles and prevent them from aggregation. An increase of temperature from 35 to 95 ^{o}C yielded significant results in terms of size and shape that altered, especially for L-aspartic acid and lactose capped CuS nanoparticles. The presence of L-alanine and lactose as capping agents in the synthesis of CuS nanoparticles yielded particles with morphologies ranging from irregular to rod-shaped. However, employing L-aspartic acid in the same materials signs of hexagonal particles were observed as the temperature reached 95 ^{o}C. In addition, when the capping agent was changed to lactose the morphology of the particles changed from rod-shaped to irregular shape.

The crystallinity of CuS nanoparticles was determined by XRD, displaying the phase of the particles as hexagonal CuS covellite phase irrespective of the capping agent used. The UV-Vis spectroscopy also confirmed the spectra of covellite CuS nanoparticles by showing the broad band in the near-IR region for all samples. For water solubility, CuS nanoparticles

prepared at 95 °C were found to be the most soluble in aqueous media as compared to the nanoparticles obtained at 35 °C and 65 °C.

Bio-functionalized ZnS nanoparticles with spherical shape were also successively synthesized. The as-prepared ZnS nanoparticles have good crystallinity and a good surface chemical environment with a narrow size distribution. The morphology of all ZnS nanoparticles formed was close to spherical shape. Determining the size of some of the nanoparticle from the TEM images was a challenge, since a sign of particles aggregation was observed. The reason behind the agglomeration is that the particles might be very small prompting an increase of the surface energy which influenced particles to aggregate. Poor particles passivation is one of the other reason that might have influenced the particles aggregation. XRD displayed the phase of the particles as cubic zinc sulfide blend for all samples. Lactose-capped ZnS nanoparticles obtained at 35 °C were more soluble in aqueous media than those obtained at 95 °C, this is because at 35 °C the size of the nanoparticles were very small and aggregated as indicated by the results obtained from TEM images.

The synthesis of FeS nanoparticles capped with either L-alanine, L-aspartic acid or lactose produced small yield with traces of impurities. The morphology of the nanoparticles was mostly dominated by close to spherical shape, with minor signs of rod-like shaped particles observed. The particles phase for FeS nanoparticles capped with either alanine or lactose, as determined by XRD, was found to be cubic greigite (Fe_3S_4) with observation of some traces of impurities, i.e., rosickyite S_8 and capping agent. In the case of FeS nanoparticles capped with aspartic acid, the absence of significant peaks demonstrated that the materials synthesized were amorphous. TEM images of all FeS nanoparticles depicted the presence of very small particles. From optical absorption measurements it was found that the band gaps showed some dependency of the temperature used in preparing the nanoparticles. Regarding water solubility, FeS nanoparticles prepared at 95 °C were found to be more water soluble

as compared to the nanoparticles obtained at 35 °C and 65 °C, with the exception of FeS nanoparticles capped with L-aspartic acid.

Toxicity results depicted particles were nontoxic at low to moderate concentrations and only induced toxicity at higher concentrations. Particles synthesized at 95 °C showed less toxicity as compared those synthesized at 35 and 65 °C. This could be attributed to fact that at higher temperature, the particles are bigger in size and cannot penetrate the cells membrane easily as compared to particles synthesized at 35 and 65 °C. However, before these particles can be applied in biological applications, several issues such as duration or time frame of detecting the toxicity of nanoparticles, and the concentration of the nanoparticles, to name a few, have to be taken into consideration. The antimicrobial properties tested positive for both Gram-positive and Gram-negative bacteria and fungi. It was found that L-alanine-capped copper sulfide nanoparticles were more effective against the bacteria than L-alanine-capped zinc sulfide nanoparticles. Overall uncapped copper sulfide nanoparticles performed better than all the particles in antimicrobial studies.

Future work and recommendations

Synthesis and characterisation of water-soluble and FeS nanoparticles:

Further synthetic strategies of making FeS nanoparticles that are water-soluble should be explored, varying certain parameters such as reaction time, pH and precursor, with alanine, aspartic acid and lactose as capping molecules. The method used in our work can also be modified by varying the solvents during preparation.

Toxicity and antimicrobial activity studies:

Although great strides have been made in the synthesis and uses of nanoparticles, there is still a significant lack of information about the impact of nanoparticles on human health and environment, especially the potential for nanoparticles toxicity. High quality organically and water soluble semiconductor nanoparticles were successfully synthesized over the past decades, however, a great need still arises for *in vitro* and *in vivo* toxicity studies to be carried out further on these particles to fully understand their bio-distribution and potential adverse effect. Since zinc is not hazardous to human body, bio-functionalized ZnS nanoparticles synthesized in this present study should be screened for its toxicity, anti-microbial and antiviral properties using different strain of microorganisms.